The mechanics of large volcanic eruptions

Agust Gudmundsson

Department of Earth Sciences, Queen's Building, Royal Holloway University of London, Egham TW20 0EX, UK (rock.fractures@googlemail.com)

Abstract

The mechanical conditions for a volcanic eruption to occur are conceptually simple: a magma-driven fracture (normally a dyke) must be able to propagate from the source to the surface. The mechanics of small to moderate (eruptive volumes less than 10 km^3) is reasonably well understood, whereas that of large eruptions (eruptive volumes of 10-1000 km^3) is poorly understood. Here I propose that, while both large and small eruptions are primarily driven by elastic energy and may come from the same magma chambers and reservoirs, the mechanisms by which the elastic energy is transformed or relaxed in these eruptions are different. More specifically, during small to moderate eruptions, the excess pressure in the source (the primary pressure driving the eruption) falls exponentially until it approaches zero, whereby the feeder-dyke closes at its contact with the source and the eruption comes to an end. Under normal conditions, the ratio of the eruptive and intrusive material of the eruption to the volume of a totally molten shallow basaltic crustal magma chamber (at the common depth of 1-5 km) is about 1400, and that of a partially molten deep-seated basaltic magma reservoir (in the lower crust or upper mantle) is about 5000. Many magma chambers are partially molten, in which case the ratio could be close to that of reservoirs. Most magma chambers are estimated to be less than about 500 km^3, for which the maximum eruptive volume would normally be about 0.4 km^3. An eruptive volume of 1 km^3 would require a totally molten chamber of about 1400 km^3. While chambers of this size certainly exist, witness the volumes of the largest eruptions, large eruptions of 10-1000 km^3 clearly require a different mechanism, namely one whereby the excess pressure maintenance during the eruption. I suggest that the primary excess-pressure maintenance mechanism is through caldera subsidence for shallow magma chambers and graben subsidence for deep-seated magma reservoirs. In this mechanism, it is the subsidence, of tectonic origin, and associated volume reduction (shrinkage) of the magma source that drives out an exceptionally large fraction of the magma in the source, thereby generating the large eruption. Most explosive eruptions that exceed volumes of about 25 km^3, and many smaller, are associated with caldera collapses. The data presented suggest that many large effusive basaltic eruptions, in Iceland, in the United States, and elsewhere, are associated with large graben subsidences In terms of the present mechanism, successful forecasting large of eruptions requires understanding and monitoring of the volcanotectonic conditions that trigger large caldera and graben subsidences.

Keywords: shallow magma chambers, deep magma reservoirs, excess pressure, caldera collapse, graben subsidence, eruption mechanics

In press in **Earth-Science Reviews**

1. Introduction

Despite great progress in volcanology in the past decades, we still cannot make reliable forecasts either to the likely eruption site or to the eruption size (volume, mass) once the eruption has started. Empirical data collected from volcanoes worldwide indicate that the volumes (or masses) of eruptive materials in volcanic eruptions are heavy-tailed (Fig. 1). This means that most of the volumes erupted from a given magma chamber (through a volcano) are comparatively small. Yet, the same magma chamber can, under certain conditions, squeeze out large volumes of magma. To know these conditions is of fundamental importance for reliable forecasting of the likely size of an imminent or beginning eruption.

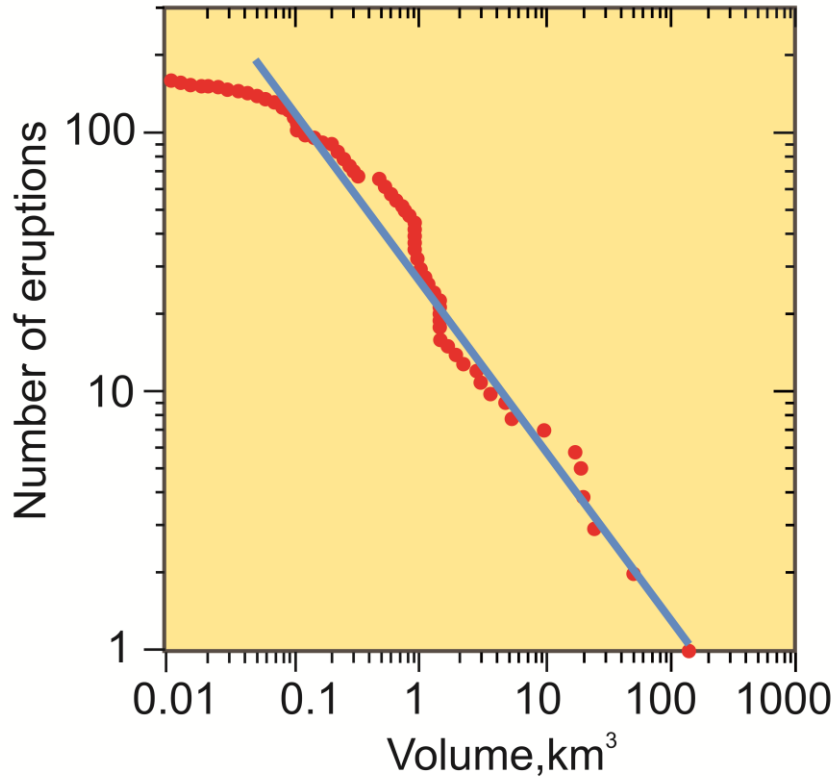

Fig. 1. *Size distribution of eruption volumes, in cubic kilometres, in relation to the number of eruptions with volumes above a certain size (modified from Pisarenko and Rodkin, 2010). The bi-logarithmic (log-log) plot shows that a straight blue line fits much of the distribution, indicating that the eruptive volume distribution follows approximately a power law. Various methods exist for testing how well one or more power laws fit such a distribution in relation to other functions (Clauset et al., 2009; Mohajeri and Gudmundsson, 2014; Gudmundsson and Mohajeri, 2013).*

Given that the conditions for volcanic eruptions are conceptually simple - a magma-driven fracture, a dyke, must be able to form a path from the source (the chamber/reservoir) to the surface – it is perhaps surprising that we cannot normally forecast the likely site of an eruption. If the crustal segment hosting a magma chamber behaved as a homogeneous and isotropic solid – an elastic half space – then all injected dykes whose magma density was similar to or less than the average density of the host rock above the chamber should reach the surface. However, crustal segments, and volcanoes in particular, do not behave as elastic

half spaces; instead they are composed of rock layers and units and contacts whose mechanical properties vary widely. As a consequence, the local stresses within the crustal segment and associate volcano show abrupt changes, resulting in complex dyke paths and many dykes becoming arrested (Gudmundsson, 2006; Galindo and Gudmundsson, 2012). The formation of a dyke path, moreover, requires energy – more specifically (fracture)

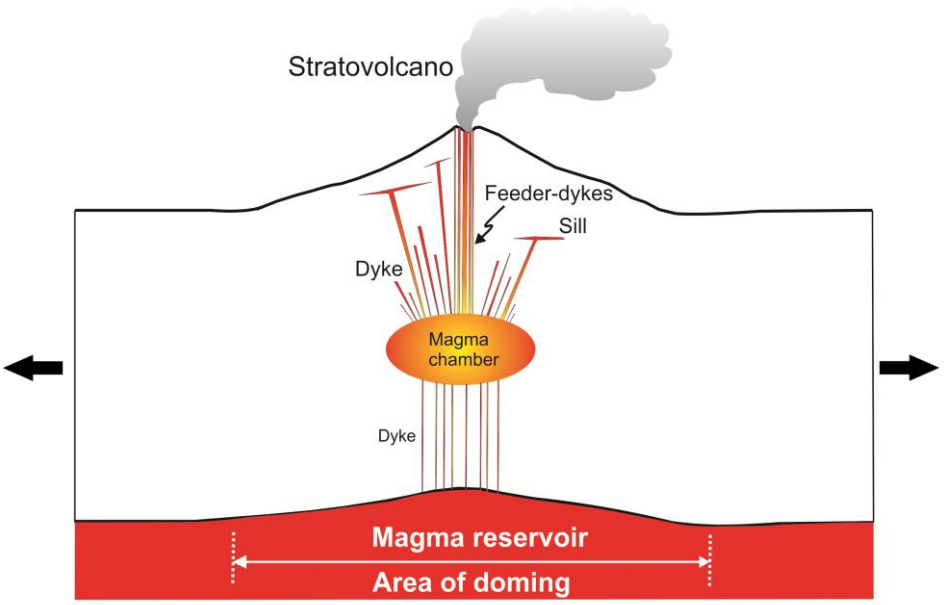

Fig. 2. *Typical magmatic plumbing system for a polygenetic or central volcano, here a stratovolcano. A deep-seated and large reservoir supplies magma to a shallow, and much smaller, magma chamber, which in turn feeds most of the eruptions of the stratovolcano. Many injected dykes from the chamber never make it to the surface but rather become arrested inside the volcano, commonly changing into sills at contacts between mechanically dissimilar rocks. Some dykes, however, supply magma to eruptions and are denoted as feeder-dykes. Magma accumulation in the deep-seated reservoir commonly results in slight doming of the crustal segment above and hosting the shallow chamber, as indicated. Such doming is one of the main mechanisms of collapse-caldera formation, particularly when the shallow magma chamber has a sill-like geometry (Gudmundsson, 2007). In addition to doming, polygenetic volcanoes may be located in fields or zones undergoing extension, such as at divergent plate boundaries, as indicated by the horizontal arrows. The crustal segment hosting the volcano is a thermodynamic system, primarily composed of the magmatic plumbing system, and its surroundings, that is, the rest of the crustal segment. The magma chamber acts as a source for the volcano and as a sink for the deeper reservoir. In the notation used in this paper, heat received by the magma chamber and work done on the magma chamber (by the surroundings) are regarded as positive.*

surface energy – and if sufficient energy is not available, the dyke-propagation path comes to an end, becomes arrested, before the dyke has a chance of reaching the surface to erupt.

Thermodynamics provides the basis for understanding the energy available to (i) propagate an injected dyke from the source to the surface to feed an eruption, and (ii) squeeze magma out of the chamber during the dyke propagation and eruption (Fig. 2). This energy, stored in the volcano and available for the two processes (i and ii), is known as elastic energy. Here the elastic energy consists of two main parts: first, the strain energy stored in the volcano before magma-chamber rupture and dyke injection, and, second, the work done

through displacement of the flanks of the volcano (or the margins of a rift zone) and the expansion and shrinkage of the magma chamber itself. Other forms of energy in volcanoes - thermal, seismic, kinetic - are important (Yokoyama, 1957; Hedervari, 1963; Verhoogen, 1989; Pyle, 1995) but less so for forming dyke paths and squeezing magma out of a chamber during an eruption.

Here I suggest that for (basaltic) eruptions in a rift zone with a deep-seated reservoir the strain energy is partly related to minor doming (Fig. 2) above the reservoir, and partly to stretching of the rift zone before rupture. The larger the reservoir, the larger is the stored strain energy before eruption. However, for the eruption to be really large, the strain energy has to accumulate in the entire crustal segment above the reservoir and there will be additional energy input into the system during the eruption because of the displacements of the boundary of the rift-zone segment (Fig. 2). This displacement is presumably one reason why feeder-dykes commonly propagate laterally at the surface following the initial fissure-segment formation. The additional energy through work goes into increasing the length and opening of the volcanic fissure/feeder-dyke, thereby allowing more magma to flow out of the chamber before it closes and the eruptions comes to an end.

For crustal segments that contain, in addition to deep-seated reservoirs, shallow crustal chambers (Fig. 2), commonly feeding stratovolcanoes, additional strain energy is stored in during inflation (expansion) of the chamber. The amount of stored strain energy depends on the mechanical properties of the crustal segment and associated volcano. In particular, more strain energy can be stored before eruption if the volcano is composed of layers with widely different mechanical properties. Thus, a stratovolcano can normally store much more strain energy, for a given size of a magma chamber and crustal segment, than a basaltic edifice. It follows that when an eruption occurs in a stratovolcano, there is normally a higher proportion of its magma that is driven out than during an eruption in a basaltic volcano. For gas-rich magma, the great compressibility of the gas may also help to maintain the excess pressure in the chamber so as to squeeze out more magma. Generally, the greater the stored strain energy before eruption, the greater is the chance of the eruption becoming large.

Really large explosive and effusive eruptions require special energy and mechanical conditions. Here I propose that these conditions are basically the same for both types of eruptions, namely subsidence of a crustal segment into a comparatively large chamber or reservoir so as to maintain the excess pressure needed to squeeze out unusually large fraction of the magma in the chamber/reservoir. The principal aim of this paper is to explore the energy and mechanical consequences of these conditions and their implications for large or great eruptions.

While large eruptions of the order of tens or hundreds of cubic kilometres are well known – some reaching thousands of cubic kilometres – and have been widely discussed, little attempt has apparently been made to explain the mechanics of such eruptions. This paper discusses the mechanical conditions for large eruptions and compares and contrasts them with the conditions for small to moderate eruptions. The paper is partly review and partly presentation of new ideas. In particular, the proposed mechanical relation between collapse-caldera formation and large explosive eruptions is partly review. By contrast, the proposed mechanical relation between graben formation or subsidence and large effusive eruptions is

new, but is shown here to be a logical extension of the mechanical ideas of collapse-driven large explosive eruptions.

2. Mechanics of 'ordinary' eruptions

To put the ideas on large eruptions, presented below, into a volcanotectonic framework, we first discuss the mechanics of small-to-medium (or moderate) eruptions. What is meant by small, moderate, or large eruptions is to some extent arbitrary. As indicated above, large eruptions are here defined as those that produce in excess of 10 km^3 of eruptive materials. But eruptive volumes (m^3 or km^3) when translated into mass (kg) depend on the density of the material. Clearly, 1 km^3 of primitive basaltic lava has much greater mass than 1 km^3 of pumice, for example. We therefore use 'magma volume equivalent', that is, the estimated volume of magma that had to flow out of the chamber/reservoir in order to generate the combined volume of eruptive and intrusive (normally dyke) materials during the eruption. We call this 'eruptive volume' and denote by V_{er}, where 'eruptive' means the fluid volume that left the chamber during the eruption. Here eruptive volumes (V_{er}) of 0.1 km^3 or less are regarded as small, those in the range of 0.1-10 km^3 are regarded as moderate, and those larger than 10 km^3 as large. It might be argued that any eruption exceeding 1 km^3 should be called large. However, given that some eruptions reach volumes of the order of 1000 km^3, I think it is better to classify eruptions of the order of 1 km^3 as moderate.

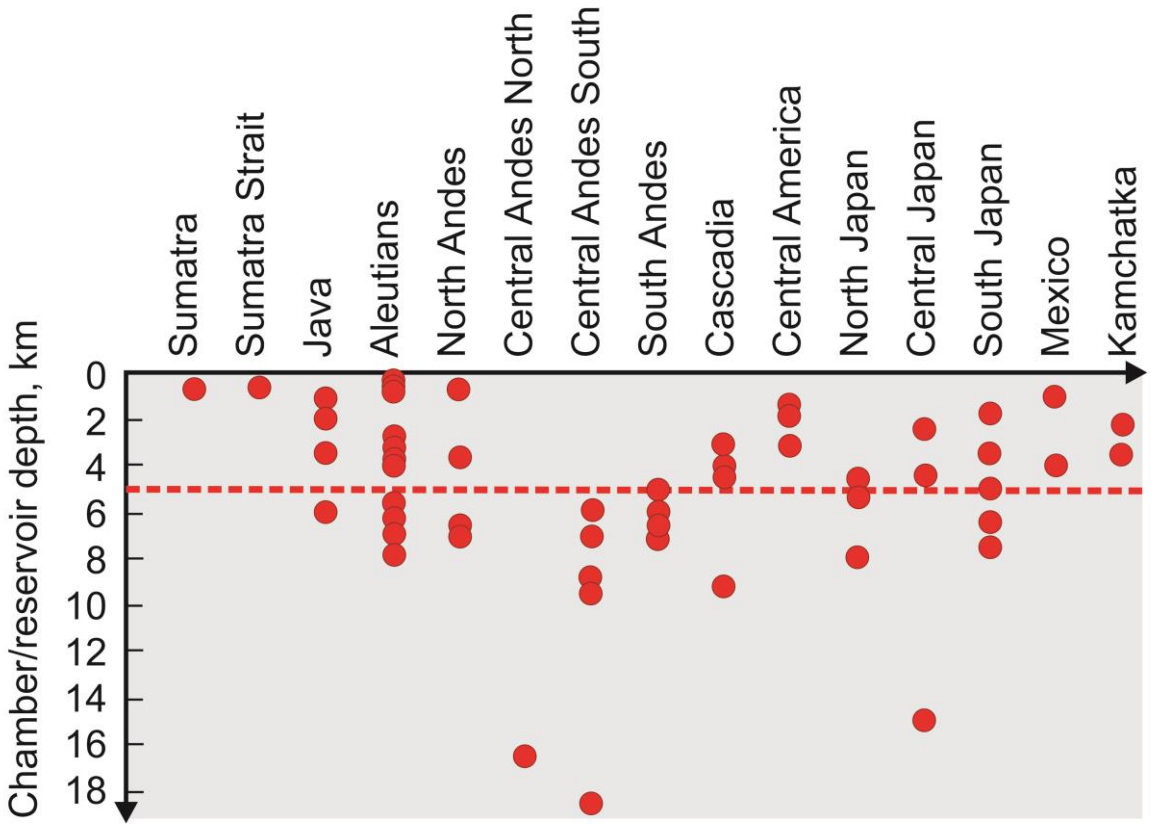

Fig. 3. *Most shallow magma chambers are in the upper part of the crust whereas deep-seated reservoirs are in the lower part of the crust, or in the upper mantle. Compilation of magma-chamber depths from 15 plate-boundary regions (Chaussard and Amelung, 2014) indicates that most of the*

shallow chambers are with roofs at depths of 0.1-5 km and mostly 1-5 km. The roofs of the deeper chambers or reservoirs, however, extend to depths of about at least 18 km. These estimates refer to chamber depths below the average regional elevation of the area or crustal segment within which the chamber is located; when referred to the depths below the tops of the associated polygenetic volcanoes themselves the depths would normally be greater, so that some reservoirs reach depths of more than 20 km below the associated volcanoes. The depths shown here are based on geodetic, seismological, and petrological/geochemical data and refer to chambers/reservoirs of 70 polygenetic volcanoes from subduction zones (arcs) in the North, Central, and South America, as well as in Sumatra and Java and Japan in Asia.

Other concepts that need definitions are those of shallow and deep-seated magma chambers. We define chambers as shallow if the uppermost contact between the host rock and the magma, that is, the roof is not deeper than 5 km. Magma chambers with roofs at greater depths, some as deep as tens of kilometres, are here classified as deep-seated and referred to as reservoirs. This classification is supported by a recent summary of magma-chamber depth ranges from many volcanic areas (Fig. 3). This distinction is to some extent arbitrary, but it is useful, particularly since most shallow magma chambers are, in fact, at depths of about 5 km or less. A shallow chamber and its deep-seated source reservoir form a 'double magma chamber'. Generally, the source reservoir is much larger than the shallow chamber to which it supplies magma. While double magma chambers are presumably the most common configuration, particularly at divergent plate boundaries, in volcanic areas where the lithosphere is very thick, such as at some convergent boundaries, there may be triple magma chambers (Fig. 3). Here, however, the focus is on double magma chambers (Fig. 2).

The principles that control the volumes injected from shallow magma chambers during 'ordinary' (mostly small and moderate) eruptions are well established. From these principles, the normal ratio between the volume of magma in the chamber and the erupted/injected magma (V_{er}) from the chamber during a particular eruption can be calculated, as is done below. First, however, we consider the volumetric flow from the chamber to the surface through the feeder-dyke (Figs. 2, 4).

The volumetric flow rate Q, in m^3s^{-1}, up through a feeder-dyke, supplying magma to an associated volcanic fissure, is normally calculated using the Navier-Stokes equation for laminar flow between parallel plates (e.g., Lamb, 1932; Milne-Thompson, 1996) as:

$$Q = \frac{\Delta u^3 W}{12\mu_m}\left[(\rho_r - \rho_m)g\sin\alpha - \frac{\partial p_e}{\partial L}\right] \quad (1)$$

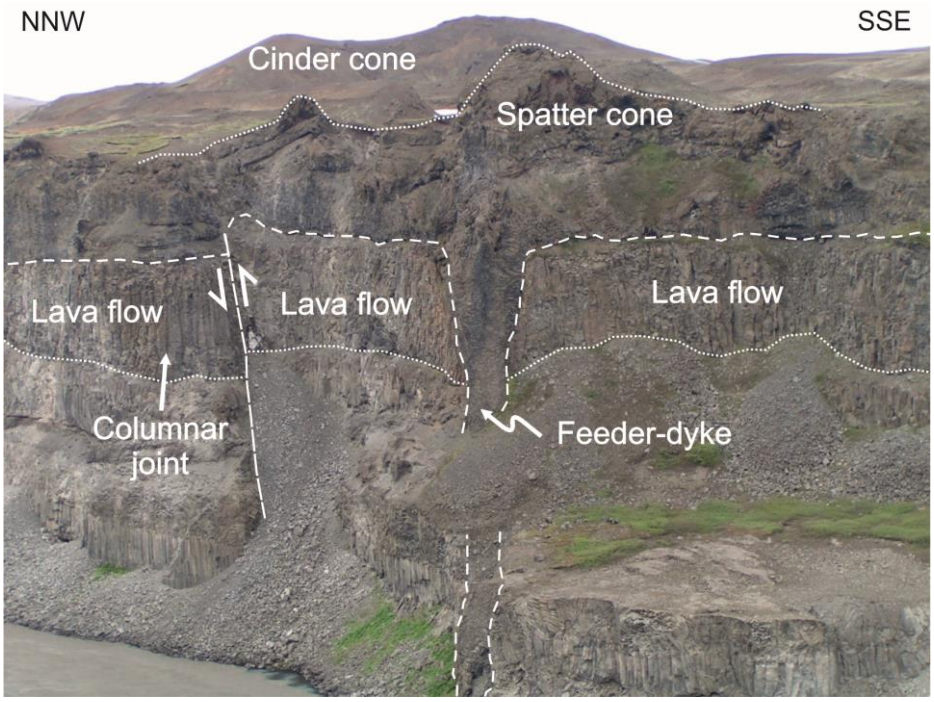

Fig. 4. *View north, part of the feeder-dyke to the 6-8000 year-old Sveinar-Randarholar crater row in North Iceland. The dyke cuts through Pleistocene lava flows with numerous columnar joints (indicated), some of which contribute to the path of the feeder, and supplied magma to spatter and cinder cones of the 75-km-long crater row. The view is across the canyon of the river Jokulsa a Fjollum, part of the river being seen in the lower left corner of the photograph. Next to the river the dyke thickness is 4.5 m but increases to 13 m where it dissects the surface (the Pleistocene lava flows) to feed the spatter cone. The magmatic overpressure of the dyke has reactivated a normal fault as a reverse fault, with a reverse slip of 5 m, located 40 m from the dyke (Gudmundsson, 2011).*

In this equation, Δu denotes the opening or aperture of the volcanic fissure or feeder-dyke, W the length or strike dimension of the fissure/feeder-dyke at the surface, μ_m the dynamic or absolute viscosity of the magma in Pa s, ρ_m the density of the magma in kg m^{-3} (assumed constant), ρ_r the average density of the crustal segment (which includes the volcano) through which the feeder-dyke propagates to the surface, g the acceleration due to gravity in m s^{-2}, α the dip of the feeder-dyke in degrees, and $\partial p_e / \partial L$ the vertical magmatic excess-pressure gradient in the direction of the magma flow, that is, in the direction of the dip dimension of the dyke, L, in metres.

The pressure driving the magma up through the feeder and to the surface derives from two sources. One is the excess pressure (p_e) in the chamber, that is, the pressure in the chamber in excess of the lithostatic pressure (or overburden pressure) in the host rock next to the chamber. At the time of magma-chamber rupture and dyke initiation, p_e is normally roughly equal to the tensile strength of the host rock, generally in the range of 0.5-9 MPa, and most commonly 2-4 MPa (Haimson and Rummel, 1982; Schultz, 1995; Gudmundsson, 2011).

The second source relates to buoyancy, that is, the density difference between the magma and the host rock through which the feeder-dyke propagates. Buoyancy is represented by the

term $(\rho_r - \rho_m)g$ in Eq. (1). Buoyancy can be positive (when magma density is less than host rock density), zero (when magma density is equal to that of the host rock), or negative (when magma density is greater than that of the host rock). The last one is common for primitive basaltic magma injected from shallow magma chambers, whereas the first one is the rule for any magma from deep-seated reservoirs (Fig. 2). Both sources contribute to the general magma overpressure (p_o) in the feeder-dyke, which is also named driving pressure and net pressure. It is the pressure that drives the propagation of all dykes (including feeder dykes), inclined sheets, and sills, as well as magma flow through conduits of different shapes, such as, in plan view, cylindrical or ellipsoidal conduits. The overpressure is defined as the total pressure minus the minimum principal compressive (maximum tensile) stress σ_3 acting on the potential dyke/sheet/sill path before magma emplacement. The overpressure may reach several tens of mega-pascals at some point along the dyke/sheet path although the excess pressure in the source magma chamber is roughly equal to the rock tensile strength and thus normally only several mega-pascals.

3. Eruption from a shallow crustal chamber

During a dyke-fed eruption, a certain volume of magma is transported from the chamber to the surface (Fig. 2). Within the framework of thermodynamics, the magma chamber may be regarded as an open thermodynamic system, whereas the crustal segment hosting the chamber, including the volcano that the chamber supplies magma to, is regarded as the surroundings of the system. Many chambers are likely to be only partially molten and behave as poroelastic bodies (e.g., Gudmundsson, 2012). Some shallow chambers, however, may be totally molten, at least for a while. Since we are interested in the maximum volume of eruptive materials that a magma chamber can produce during an 'ordinary' eruption, we shall here assume the chamber to be totally molten. In case of a partially molten chamber, the host-rock compressibility (β_r) can be substituted with pore compressibility. The volume of magma V_{er} erupted or transported from a totally fluid magma chamber by a feeder-dyke to the surface (and including the volume of the feeder itself) during an eruption may be estimated as follows (e.g., Gudmundsson, 1987a):

$$V_{er} = p_e(\beta_r + \beta_m)V_t \qquad (2)$$

Here p_e denotes the magma excess pressure (with the unit of Pa), β_m the magma compressibility and β_r the host-rock compressibility (both with the unit of Pa^{-1}), and V_t the total volume of the chamber. Transport of magma out of the chamber—through the feeder-dyke—stops and the eruption comes to an end when the excess pressure becomes so small ($p_e \rightarrow 0$) as to be unable to keep the dyke-fracture open (particularly for feeders of low-viscosity basaltic magma) at its contact with the chamber (Fig. 2).

Let us now estimated the percentage of the magma that could leave the chamber in an eruption before the feeder-dyke would close at its contact with the chamber. Based on data from Murase and McBirney (1973), the static compressibility β_m for tholeiite (basaltic) magma at 1100-1300ºC is estimated at around $1 \times 10^{-10} Pa^{-1}$ (Gudmundsson, 1987a).

Similarly, for a shallow chamber, the host-rock compressibility β_r is estimated at about 2.94 × 10^{-11}Pa^{-1}, for a dynamic/static compressibility ratio of 2.0. For a shallow magma chamber located in a highly fractured crust, as is common, a more reasonable dynamic/static ratio might be 10 (Gudmundsson, 2011), in which case the compressibility β_r is estimated at 1.47 × 10^{-10}Pa^{-1}. For an in-situ tensile strength of 0.5-9 MPa (Gudmundsson, 2011), taken as equal to p_e, Eq. (2) gives the ratio of the eruptive volume V_{er} to the total volume of the chamber V_t from about 2.45 × 10^{-3} (for p_e = 9 MPa) to about 1.36 × 10^{-4} (for p_e = 0.5 MPa). For a

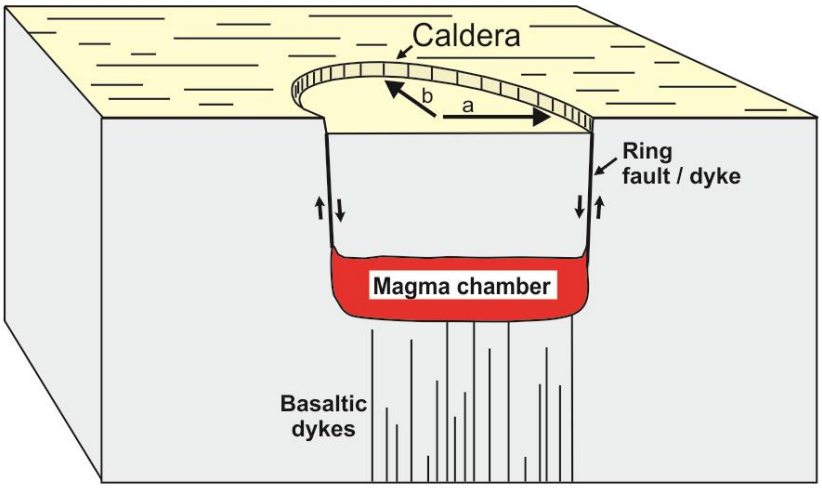

Fig. 5. *Many collapse calderas have close to vertical ring-faults. In plan view, however, most ring-faults are not perfect circles but rather ellipses with the semi-major axis a somewhat larger than the semi-minor axis b. Some ring-faults are injected by ring-dykes, whereas others are not.*

common in tensile strength of 4 MPa (so that p_e = 4 MPa), we get the approximate general ratio of:

$$V_{er} \approx 7 \times 10^{-4} V_t \qquad (3)$$

which implies that, typically, less than 0.1% (here, 0.07%) of the volume of a totally fluid basaltic magma chamber would be erupted/injected during an ordinary eruption.

Eruption volumes can basically be as small as one likes to record. However, typical 'small' eruptions may be regarded as 0.01-0.1 km^3 (Fig. 1). These are common values for small basaltic (to andesitic) eruptions in central volcanoes (stratovolcanoes and calderas) such as in Iceland (Gudmundsson, 1987a; Thordarson and Larsen, 2007; Thordarson and Höskuldsson, 2008) and elsewhere. For an eruption of 0.01 km^3, assuming that the inflow of magma is so slow during the eruption itself that it can be neglected—as is usually justified (Gudmundsson, 2012)—then, from the approximate Eq. (3), the magma-chamber volume needed to supply magma to the eruption would be 10 km^3. Similarly, for an eruptive volume of 0.1 km^3, the volume of the source chamber would be 100 km^3.

Caldera areas are a good indication of the plan-view (lateral cross-sectional) areas of the associated magma chambers at the time of caldera formation (Fig. 5). Normally, however, the

caldera area is somewhat smaller than the cross-sectional area of the magma chamber, particularly for outward-dipping ring faults (discussed below), but is nevertheless a good proxy to the chamber area when the caldera collapsed (Gudmundsson, 1998; Roche and Druitt, 2001; Holohan et al., 2005; Kusumoto and Takemura, 2005; Acocella, 2007; Gudmundsson, 2007, 2015; Kusumoto and Gudmundsson, 2009; Gregg et al., 2012; Geyer and Marti, 2014). This is particularly so because many ring-faults appear to be close to vertical (Fig. 5). A typical caldera in the neovolcanic zone in Iceland has an area of about 50 km^2, the largest reaching about 180 km^2. For a totally molten 10 km^3 magma chamber with a (assumed circular) cross-sectional area of 50 km^2, the chamber thickness would be around 0.2 km, or 200 m. Sills of similar thicknesses and with the potential of developing into magma chambers are well known in the lava pile in Iceland and elsewhere (Gudmundsson, 2012). For a totally molten 100 km^3 magma chamber with a cross-sectional area of 50 km^2, the chamber thickness would be around 2 km. Again, plutons of this and greater thicknesses are known or inferred from several deeply eroded, extinct central volcanoes in Iceland (Gudmundsson, 2012) and elsewhere. Perhaps the best-known sill-like (or somewhat laccolith-like) exposed magma chamber of this thickness, however, is the Torres del Paine fossil magma chamber in Chile (Michel et al., 2008). That chamber/pluton is primarily of granite, is formed in many magma injections, and has maximum thickness is about 2 km. Most magma shallow magma chambers appear to grow incrementally, that is, through many (often sill-like) magma injections (e.g., Gudmundsson, 1990; de Silva and Gosnold, 2007; Annen, 2011).

The overall compressibility of intermediate magma (Murase and McBirney, 1973) and acid magma (Kress and Carmichael, 1991; Dobran, 2001), including the effects of water and carbon dioxide in the magma, are not much different from that of basaltic magmas. Volatile content, however, can have significant effects on magma compressibility (Blake, 1984; Ochs and Lange, 1997; Woods and Huppert, 2003; Malfait et al., 2011; Guo, 2013; Seifert, 2013). Gas generally has much higher compressibility than either liquids or solids. Thus, gas bubbles in magma have a much higher compressibility than either the magmatic liquid itself or the solid host rock. The main volatiles are water, H_2O, and carbon dioxide, CO_2, whereas sulphur (as H_2S and SO_2) is also common (e.g., Gonnermann and Manga, 2013). Here we focus on water and carbon dioxide since these are the main volatiles.

The main difference between water and carbon dioxide as regards their mechanical effects in shallow magma chambers is that most of the CO_2 exsolves to form bubbles at much greater depths (higher total pressure) than does H_2O (Gonnermann and Manga, 2013). In particular, CO_2 exsolution and bubble formation occurs in acid magma (rhyolite) at pressures up to and in excess of 100 MPa, and for basaltic magma at pressures up to and in excess of 25 MPa. By contrast, H_2O exsolves in acid magma at total pressures less than 100 MPa, and in basaltic magma at total pressures less than 25 MPa. In the uppermost part of volcanic zones worldwide the average crustal density is about 2500-2600 kg m^{-3}, so that 25 MPa corresponds to roughly 1 km depth, and 100 MPa to about 4 km depth. Many, perhaps most, shallow magma chambers are in roughly this depth range (Fig. 3). Thus, generally, for many shallow chambers much of CO_2 (and some H_2O) in acid magmas is readily exsolved and forms bubbles. Since bubbles in acid magma have negligible mobility, they would remain in the

magma, except in the case of vigorous convection, in which case the gas could accumulate at the top of the acid magma and form a separate phase.

By contrast, exsolution and bubble formation is not expected in basaltic magmas at the depth of most shallow magma chambers. Thus, much of the gas exsolution in basaltic magma takes place at very shallow depths, particularly in feeder-dykes when the magma is on its path to the surface (Fig. 4). This agrees with field studies. In Hawaii, for example, studies indicate that most of the exsolution of gas in basaltic magmas occurs in the uppermost few hundred metres of the feeder/conduit (Greenland et al., 1985, 1988). Similar results are obtained through direct observations of dykes, sills, and inclined sheets in deeply eroded lava piles and central volcanoes. Most sheet-like intrusions show only small and rather infrequent vesicles (formed by expanding gas) at depths exceeding several hundred below the original surface of the volcanic zone/central volcano. By contrast, some feeder-dykes contain large vesicles close to the surface (Galindo and Gudmundsson, 2012).

The potential effects of exsolution in magma chambers on the compressibility of magma depend on the fraction of gas in the magma. The compressibility of the gas may be 10^2-10^3-times the compressibility of liquid magma (Woods and Huppert, 2003; Malfait et al., 2011; Guo, 2013; Seifert, 2013). Thus, the gas bubbles are much more compressible than the liquid magma and the associated crystals. However, the overall compressibility of the magma plus gas depends on the gas fraction. For small volume-fraction of gas in the chamber, the compressibility of the liquid magma (β_m) dominates over the compressibility of gas (β_g), so that the effect of the bubbles on the overall compressibility of the magma (gas plus liquid) is small. By contrast, when the volume fraction of gas in the magma becomes larger than the β_g / β_m ratio then the high compressibility of the gas bubbles start to increase significantly the overall compressibility of the liquid magma plus gas in the chamber (Woods and Huppert, 2003). Even when the volume fraction of gas becomes high, the bubble-rich and highly compressible parts of the magma chamber are likely to be confined to certain layers or compartments (Gudmundsson, 2012), rather than being uniformly distributed in the chamber. This implies that the compressibility of the magma chamber is likely to be highly heterogeneous, so that within the chamber there may be layers or compartments with high compressibility and others with much lower compressibility, resulting in uneven volume changes and overall response of different magma-chamber compartments to volume decrease during eruptions. In this paper, however, we consider only the compressibility of the magma in the chamber as a whole.

Based on the above considerations, a very gas-rich acid magma where the gas forms a separate phase in a shallow magma chamber would have a much higher compressibility than basaltic magma, perhaps by several orders of magnitude. Depending on the amount of acid magma in the chamber and the chamber configuration – for example, whether the chamber is layered with the evolved magma on the top of the mafic magma or composed of compartments with different gas content - the compressibility of gas-rich acid magma (gas plus liquid) can be at least 10 and possibly 100 times that of a chamber composed entirely of basaltic magma (cf. Woods and Huppert, 2003).

For such a high magma compressibility, we have $\beta_m >> \beta_r$, in which case Eq. (2) reduces to:

$$V_{er} = p_e \beta_m V_t \quad (4)$$

Equation (4) has commonly been used (Machado, 1974; Blake, 1981; Wadge, 1981) and implies that the ratio of erupted/intruded magma from the chamber to the total magma volume in the chamber depends almost entirely on the magma compressibility β_m. For a purely acid bubble-rich magma in a chamber, using p_e = 4 MPa and β_m = 10^{-8} Pa^{-1} (100-times higher than for tholeiite magma) the ratio in Eq. (4) would then reach the maximum value of:

$$V_{er} \approx 4 \times 10^{-2} V_t \quad (5)$$

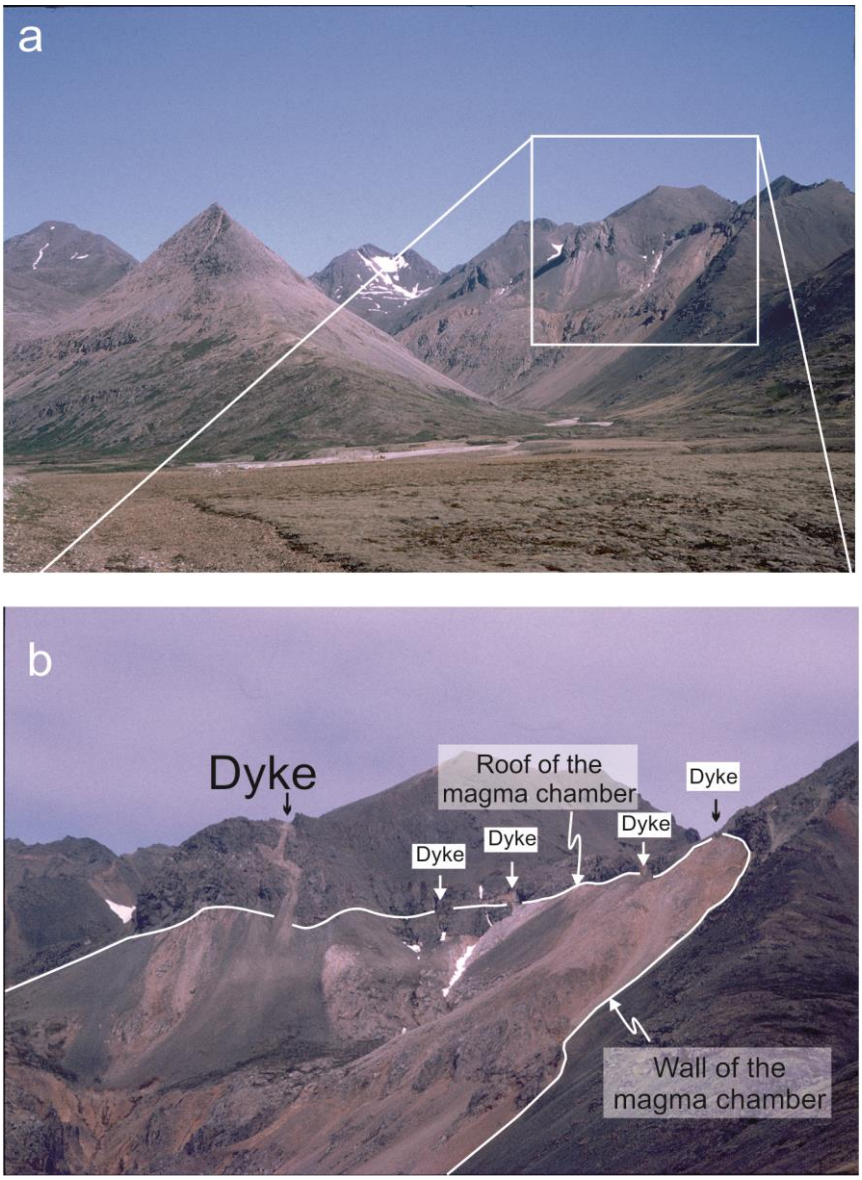

Fig. 6. *View northwest, part of the extinct Slaufrudalur shallow magma chamber (pluton), composed of granophyre, in Southeast Iceland. The pluton is 6.5–10 Ma, has an exposed area of 15 km^2, and is*

the second largest pluton/fossil magma chamber in Iceland. a) Part of the roof and a wall of the fossil magma chamber are exposed in the valley of Slaufrudalur, the peak to the left being Bleikitindur. The maximum depth of erosion is about 2 km below the initial top of the associated volcano to which the chamber acted as a source. b) Close-up of part of (a) showing many granophyre dykes (some indicated by arrows) dissecting the host-rock roof, composed of basaltic lava flows.

so that as much as 4% of the magma in the acid chamber (or the bubble-rich acid compartment of a larger chamber) could leave the chamber (as intrusive and extrusive material) during an eruption.

If we compare this maximum percentage with the well-documented postglacial acid eruptions in Iceland, we can get a crude idea of the sizes of the acid source magma chambers (or acid compartments). For the 38 postglacial 'dry' explosive acid eruptions in Iceland, the volume range is from 0.1 km^3 to about 3.3 km^3 (Thordarson and Hoskuldsson, 2008). An eruptive volume of 0.1 km^3 would, according to Eq. (5), require a magma chamber of only 2.5 km^3, whereas an eruptive volume of 3.3 km^3 would require chamber of around 83 km^3. Chambers, or acid compartments, of these sizes can certainly exist in the active volcanic zone of Iceland. For the typical chamber cross-sectional area (based on typical caldera areas) of 50 km^2, the 2.5 km^3 chamber would need to be only 50 m thick, most likely a sill-like chamber. By contrast, the 83 km^3 chamber would need to be about 1.7 km thick. While this would be thick for an acid magma chamber, it is only about double the thickness of the exposed part of the Slaufrudalur acid magma chamber in Southeast Iceland—a chamber/pluton with an exposed acid volume of about 10 km^3 (Fig. 6).

4. Eruption from a deep-seated magma reservoir

Deep-seated reservoirs are magma sources located in the lower crust or upper mantle (Figs. 2 and 3). The reservoirs supply magma (mostly basaltic or andesitic) either directly to the surface or, alternatively, to shallow magma chambers (Figs. 2, 5, and 6). Together a shallow magma chamber and its deep-seated source reservoir form a double magma chamber, of the type common at many plate boundaries (Gudmundsson, 2006).

Magma reservoirs are normally partially molten, that is, they behave as poroelastic media. They are deeper than 5 km, by definition, and mostly in the depth range of 6-20 km (Fig. 3), although some may be as deep as 25-30 km or more. Based on typical crustal-rock densities (e.g., Gudmundsson, 2011) the vertical stresses or total pressures at the location of the reservoirs are thus normally in excess of 150 MPa, and commonly 200-500 MPa. It follows that, generally, neither acid magma, which might be produced at the top of a reservoir, nor andesitic and basaltic magmas, which constitute their bulk magmas, would be subject to exsolution of CO_2 or H_2O. The compressibility of the magma or melt in a typical deep-seated reservoir is thus normally not affected by bubble formation.

For a poroelastic magma reservoir filled with magma or melt, four compressibilities come into play (Bear, 1972; cf. Wang, 2000), here defined assuming isothermal conditions. The first one is the bulk compressibility β_b. A measure of the fractional change in the bulk volume ΔV_b of the entire poroelastic reservoir due to change in magmatic excess pressure Δp_e, bulk compressibility is defined as (Bear, 1972):

$$\beta_b = \frac{\Delta V_b}{\Delta p_e V_b} \tag{6}$$

where V_b is the original volume of the poroelastic reservoir. When Δp_e is positive, so that the excess pressure in the reservoir increases, then the reservoir expands, that is, its bulk volume change ΔV_b is positive. The second is the solid matrix compressibility β_s. A measure of the fractional change in volume of the solid matrix ΔV_s of the reservoir (the crystal mush) when the excess pressure changes, the solid matrix compressibility is defined as (Bear, 1972):

$$\beta_s = -\frac{\Delta V_s}{\Delta p_e V_s} \tag{7}$$

where V_s is the original volume of the matrix of the reservoir. When Δp_e is positive, so that the excess pressure in the reservoir increases, the matrix shrinks, that is, its volume decreases, hence the negative sign in Eq. (7). The third is the pore compressibility β_p. A measure of the fractional change in the pore volume ΔV_p (the volume occupied by the magma) when the excess pressure changes, the pore compressibility is defined as (Bear, 1972):

$$\beta_p = \frac{\Delta V_p}{\Delta p_e V_p} \tag{8}$$

where V_p is the original pore volume (magma volume) in the reservoir. When Δp_e is positive, so that the excess pressure in the reservoir increases, the pores holding the magma expand and the pore volume increases. The fourth is magma (melt or fluid) compressibility β_m. A measure of the fractional change in magma volume ΔV_m (and inversely a measure of magma density) when the excess pressure changes, the magma compressibility is defined as (Bear, 1972):

$$\beta_m = -\frac{\Delta V_m}{\Delta p_e V_m} \tag{9}$$

where V_m is the original magma volume in the reservoir. When new magma is added to the reservoir, so that the excess pressure Δp_e increases, part of the volume needed for the new magma is obtained by compressing (and increasing the density of) the existing (original) magma in the pore space of the reservoir, hence the negative sign in Eq. (9).

These compressibilities can now be combined to give the ratio of the reservoir volume to the eruptive volume during ‘ordinary’ poroelastic eruptions from reservoirs (Fig. 2). This is

done by noticing first that the bulk compressibility and the solid matrix compressibility are related as follows (Bear, 1972):

$$\beta_b = (1-\phi)\beta_s + \phi\beta_p \tag{10}$$

where ϕ is the porosity (magma or melt fraction) of the reservoir. Because the solid grains of the matrix are stiffer (have a higher effective Young's modulus) than the pores, we have $(1-\phi)\beta_s << \beta_p$, in which case Eq. (10) reduces to:

$$\beta_b = \phi\beta_p \tag{11}$$

As indicated above, when the reservoir receives new magma or melt from the mantle, part of the volume needed for the new magma is obtained by compressing the existing magma, and part by expanding the pores containing the magma. Which one dominates, pore expansion or magma compression, depends on the ratio of the respective compressibilities, that is, the ratio β_m / β_p. More specifically, if magma or melt of volume ΔV_m is added to the reservoir of original total pore or magma volume $V_m (=V_p)$, then the increase in excess pressure Δp_e is given by:

$$\Delta p_e = \frac{\Delta V_m}{V_m \beta_m}\left(1 - \frac{\beta_p}{\beta_m + \beta_p}\right) \tag{12}$$

Eq. (12) can then be simplified further, so as to obtain:

$$\Delta p_e = \frac{\Delta V_m}{V_m(\beta_m + \beta_p)} \tag{13}$$

Using the notation in Eqs. (2-5), the eruptive volume V_{er} denotes the magma volume leaving the reservoir and thus includes the intrusive material (dykes, inclined sheets) as well as the proper eruptive material (the material reaching the surface as lava flows, pyroclastics, etc). Making the reasonable assumption that the reservoir was in mechanical (lithostatic) equilibrium with its surrounding, so that $p_e = 0$ (the excess pressure is zero), before the addition of magma of volume ΔV_m to the reservoir, we can then equate ΔV_m with the eruptive volume, in which case $\Delta V_m = V_{er}$. Using ϕ for reservoir porosity, we have:

$$V_m = V_p = \phi V_b \tag{14}$$

From the considerations above and Eqs. (13, 14) the bulk volume of the reservoir V_b can be obtained from the following equation:

$$V_b = \frac{V_{er}}{p_e \phi (\beta_m + \beta_p)} \tag{15}$$

We can now use Eq. (15) to obtain typical ratios between the bulk volume of a reservoir and its eruptive volume during an ordinary eruption. The condition for reservoir rupture and dyke (the potential feeder) injection is (Gudmundsson, 2011):

$$p_l + p_e = \sigma_3 + T_0 \tag{16}$$

where p_l is the lithostatic pressure (equal to overburden pressure or vertical stress when the reservoir is mechanical or lithostatic equilibrium with its surroundings), σ_3 is the minimum compressive (maximum tensile) principal stress, and T_0 is the in-situ tensile strength of the host rock of the reservoir. When the reservoir is in lithostatic equilibrium and before new magma enters it, we have $p_l = \sigma_3$. Thus, for rupture and dyke injection to occur (when magma of volume ΔV_m is added to the reservoir), then $p_e = T_0$, that is, the excess pressure at rupture is roughly equal to the tensile strength of the host rock (more specifically the roof rock) of the reservoir.

While the in-situ tensile strength varies from 0.5 to 9 MPa (Gudmundsson, 2011), we shall here use the same typical (average) value as in Eqs. (2-5), namely 4 MPa. From the discussion above, and the results obtained by Murase and McBirney (1973), we estimate the magma compressibility β_m for tholeiite (basaltic) magma at 1100-1300ºC the same as for the shallow chamber, namely as 1×10^{-10}Pa^{-1}. For a deep-seated reservoir associated with the volcanic zones of Iceland (Gudmundsson, 1987a), we estimate the pore compressibility as about 9×10^{-11} Pa^{-1} and the average porosity as 0.25 (25%). Both these values are poorly constrained and could easily vary by a factor of 2. In fact, it is possible that the topmost part of a reservoir is totally molten, but here we shall use the more general model where the reservoir is partially molten. Using these values, Eq. (15) gives the following ratio between the bulk volume of the reservoir V_b and the eruptive volume in an ordinary poroelastic eruption V_{er} as:

$$V_{er} \approx 2 \times 10^{-4} V_b \tag{17}$$

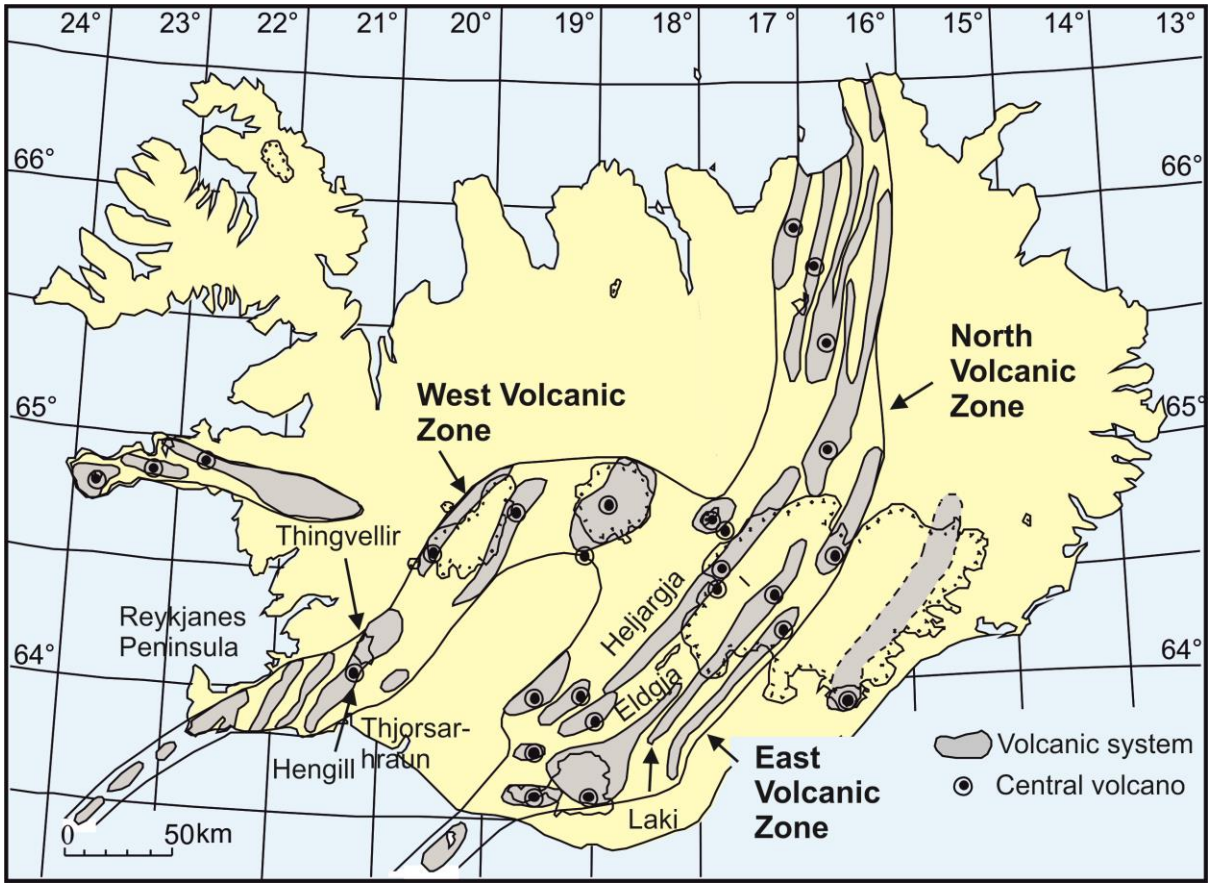

Fig. 7. *Map of Iceland showing the main volcanic zones and systems (modified from Gudmundsson, 2006). The West, North, and East volcanic zones are shown (the zone on the peninsula to the west is the Snaefellsnes Zone, which is not referred to in the text). The volcanic systems are of Holocene age and composed of swarms of tectonic fractures (mostly normal faults and tension fractures) and volcanic fissures at the surface, and dykes and normal faults at greater depths. Most systems contain, in addition, a polygenetic volcano, a central volcano, which is either a stratovolcano or a collapse caldera. Also located are the grabens of Thingvellir, Heljargja, and Eldgja (Eldgja also being a volcanic fissure), the Laki volcanic fissure or crater row, the southernmost part of the Thjorsarhraun lava flow, the Hengill Volcano, and the Reykjanes Peninsula.*

Let us now apply this to typical eruptions from deep-seated reservoirs, again using well-documented results from Iceland. The Holocene volcanic fissures on the Reykjanes Peninsula (Fig. 7) in Southwest Iceland are mainly derived from deep-seated reservoirs (Fig. 8). This follows because there are no known shallow magma chambers on the peninsula (Andrew and Gudmundsson, 2007). These are mainly tholeiite basalts and have an average eruptive volume of about 0.11 km^3 (Gudmundsson, 1986). The depth to the magma reservoirs beneath

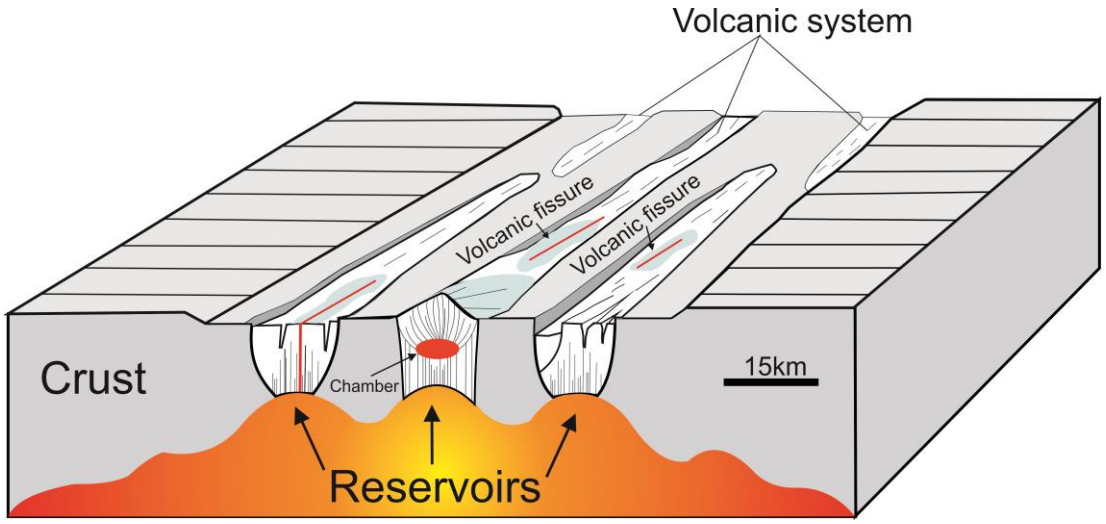

Fig. 8. *Cross-section through typical volcanic systems in rift zones (such as at divergent plate boundaries). Here only one of the systems has a shallow chamber and, consequently, a polygenetic (central) volcano. The volcanic fissures (and feeder-dykes) in the other systems are fed directly from deep-seated reservoirs. Some volcanic systems in Iceland (such as on the Reykjanes Peninsula, Fig. 7), and apparently most systems at most slow-spreading ridges, lack shallow magma chambers and are thus supplied with magma directly from reservoirs in the lower crust or upper mantle.*

the Reykjanes Peninsula may be anywhere between 10 km and 20 km. The crustal thickness, however, is only 11-12 km (Brandsdottir and Menke, 2008), so that we take the reservoirs to be at 12 km depth. The average length of the volcanic fissures (the feeder-dykes at the surface) on the Reykjanes Peninsula is 2.2 km, and with the indicated depth to the reservoir the feeder-dyke height or dip dimension is 12 km. For a feeder-dyke of these dimensions, the classic fracture mechanics equations would indicate a surface thickness of about 4 m (cf. Gudmundsson, 2011; Becerril et al., 2013), a common thickness of dykes in regional swarms in Iceland (Gudmundsson, 2006).

For these dimensions, the dyke volume would be around 0.1 km^3, so that the total volume of magma injected from the reservoir during the average eruption would be about 0.2 km^3. From Eq. (17) the corresponding source reservoir would be around 1000 km^3. The estimated average cross-sectional areas of the Holocene volcanic systems that supply magma to the fissure eruptions on the Reykjanes Peninsula (Figs. 7 and 8) is about 480 km^2 (Gudmundsson, 1986). The cross-sectional areas of the source reservoirs are likely to be similar, in which case a reservoir with thickness of just over 2 km would be sufficient to supply magma to the average volcanic fissure. Given the likely dimensions of the reservoirs, such a thickness is very reasonable, so that the fissure eruptions do not pose any reservoir volume problems as regards the ordinary poroelastic mechanism.

Holocene lava shields—(mostly) monogenetic ‘small’ shield volcanoes—are also common on the Reykjanes Peninsula and elsewhere in Iceland (Figs. 9 and 10). The shields all have very primitive composition (picrite basalt to olivine tholeiite) and known to come from deep-seated magma reservoirs, both on the Reykjanes Peninsula as well as elsewhere (Rossi, 1996; Andrew and Gudmundsson, 2007). If we consider first the shields on the Reykjanes Peninsula, then most of these are small – with volumes of less than 0.75 km^3

(Gudmundsson, 1986). The feeder-dykes for the shields come from deeper (more primitive) parts of the reservoirs (Fig. 9) than the fissure eruptions (which mostly produce more evolved tholeiite). Using 15 km for the dyke dip dimension and the same dyke length and thickness as above, a feeder-dyke volume of about 0.13 km^3 is added to the typical shield volume of 0.75 km^3, bringing the total to about 0.9 km^3. From Eq. (17) the bulk volume of the corresponding reservoir would have to be about 4500 km^3. For the reservoir of cross-sectional area of 480

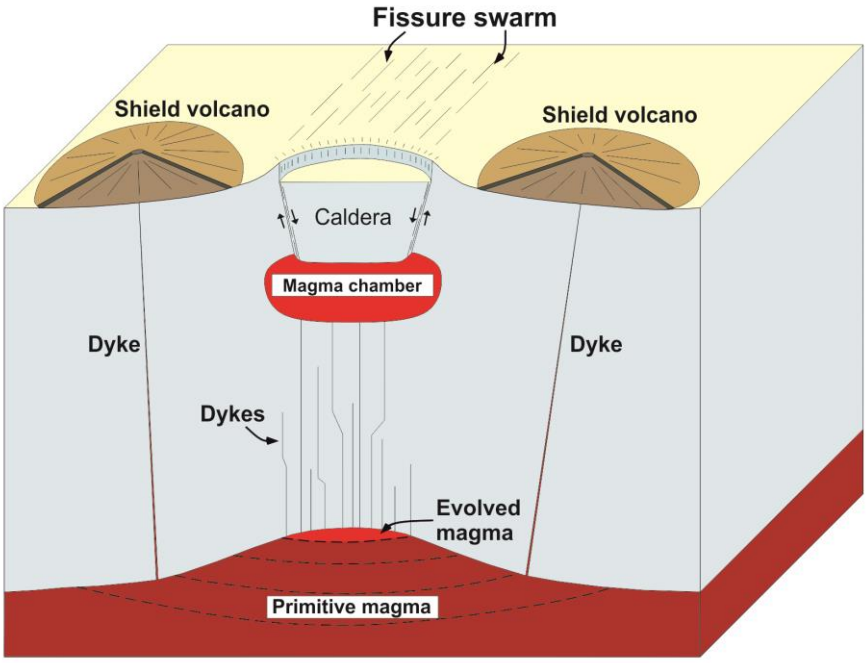

Fig. 9. *Monogenetic lava shields (cf. Fig. 10) are of primitive basalts that are normally derived directly from deep-seated reservoirs, particularly their marginal parts. Depending on its depth, absence or presence of convection, and other conditions, a reservoir may become density stratified with the more evolved (and usually less dense) magmas collecting in the upper part and the more primitive magmas in the deeper and marginal parts of the reservoir. Together the caldera (a central volcano) and the fissure swarm constitute a volcanic system (Figs. 7 and 8). In a rift zone, such systems tend to be elongated, but outside rift zones (e.g., at many convergent boundaries) they may be more equidimensional, such as circular or square-shaped.*

km^2, as used above, the thickness of the reservoir to produce 0.9 km^3 would have to be about 9.4 km (Figs. 8 and 9).

A thickness of 9 km for a deep-seated reservoir is quite possible, and some may in fact be thicker. Furthermore, most of the Holocene lava shields in Iceland formed early in Holocene when the glacial rebound effects very likely resulted in, temporarily, more extensive reservoirs and their higher melt fraction or porosity (Andrew and Gudmundsson, 2007). Thus, a thinner reservoir with a higher porosity could have generated shields of these volumes.

Much larger eruptions than those mentioned above have occurred in Iceland. Among large fissure eruptions, presumably fed by deep reservoirs, are the 934 Eldgja eruption (20 km^3), the 1783 Laki eruption (15 km^3), as well as the Thjorsa lava eruption (25 km^3), which occurred about 8600 years ago (Fig. 7; Thordarson and Höskuldsson, 2008). Similarly,

several of the Holocene lava shields reach tens of cubic kilometres, including Trölladyngja and Skjaldbreidur (Fig. 10), with estimated volumes of 15-20 km^3 (Rossi, 1996). From Eq. (17) eruptive volumes in a single eruption of 20 km^3 would require a reservoir of 100,000 km^3. The areas of the largest volcanic systems in Iceland are 2300-2500 km^2 (Thordarson and Höskuldsson, 2008), and some of the large lava shields are associated with systems of this size. If the cross-sectional areas of the associated reservoirs are similar in size, then their thicknesses would have to reach some 40 km. This is a very great thickness, and generally unlikely for typical fissure-feeding reservoirs (Gudmundsson, 1986, 1987a). Glacial rebound effects and increased melt fraction may certainly have contributed to the formation of the large lava shields in early Holocene (Andrew and Gudmundsson, 2007), as well as to the generation of the Thorsa lava some 8600 years ago (Fig. 7). But there are no known rebound effects that could help explain the large volumes of the 934 Eldgja or the 1783 Laki lava flows (Fig. 7). The chemical differences between these lava flows indicate that they come from separate reservoirs (Thordarsson and Larsen, 2007).

Fig. 10. *View east, the lava shield Skjaldbreidur in the West Volcanic Zone of Iceland (Figs. 7 and 16). Skjaldbreidur formed some 9,000 years ago and has an estimated volume of about 15 km^3.*

5. Excess pressure change in a chamber/reservoir during an ordinary eruption

Whether or not lava flows of 15-25 km^3 could form in ordinary poroelastic eruptions through the mechanism discussed above depends on the size and melt fraction of the reservoir. For Iceland these are comparatively large eruptions, although common in the Pliocene and Pleistocene lava pile. There is of course plenty of magma beneath Iceland. The main problem as regards the ordinary mechanism is how to squeeze large volumes of magma out of the

reservoir/chamber in a single eruption before the excess pressure in the reservoir/chamber becomes zero and the feeder-dyke closes at its contact with the source.

For simplification, consider the transport of basaltic magma through a feeder (Eq. 1; Figs. 2 and 4) whose source is a totally molten shallow magma chamber. We consider the case where the host rock and magma densities are equal so that $(\rho_r - \rho_m)gL$ = 0 in Eq. (1) and the magma is driven up through the feeder-dyke solely by the excess-pressure gradient, $\partial p_e / \partial L$ in Eq. (1). This assumption can easily be relaxed, as well as the assumptions of a totally molten chamber (the analysis can be extended to a partially molten reservoir), but is made here because the main point is the excess-pressure variation in the chamber itself and its effect on closing the feeder at its contact with the source, thereby bringing the eruption to an end. How rapidly the excess pressure in the chamber becomes zero determines the duration of the eruption and, partly, its volume.

During dyke injection and magma transport to the surface (Figs. 2, 4 and 6), the excess pressure in the source chamber decreases if (a) there is not enough gas exsolution or other processes operating to maintain the excess pressure or (b) volumetric flow rate of new magma into the chamber is much lower than the flow rate out of the chamber/reservoir and to the surface. As indicated above, gas exsolution is unlikely to contribute significantly to excess pressure in shallow basaltic chambers, and certainly not in deep-seated basaltic

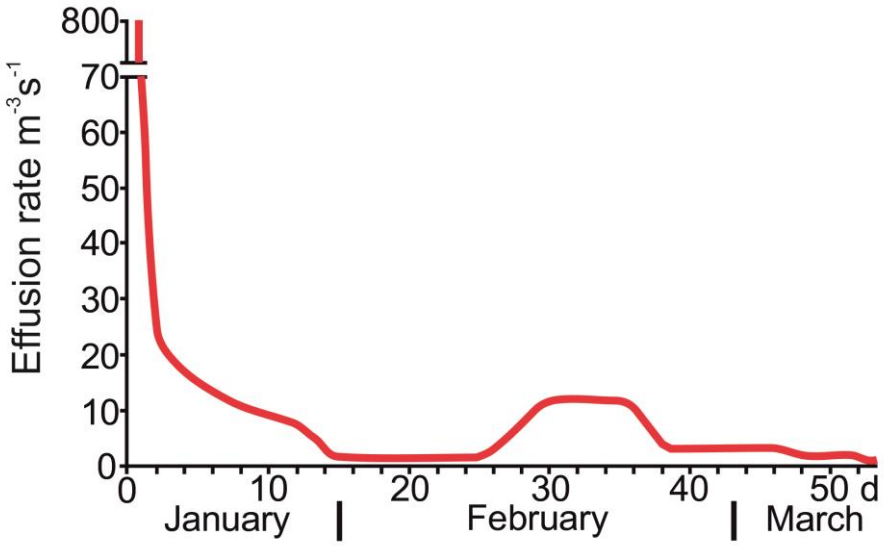

Fig. 11. *Volumetric flow (effusion) rate as a function of time during the 1991 Hekla eruption in Iceland (cf. Galindo and Gudmundsson, 2012). There is an abrupt increase in the rate in February, which is here thought to be related to a small increase in the opening (aperture) of the feeder-dyke, in accordance with the cubic law (Eq. 1).*

reservoirs. Geodetic data indicate that during basaltic eruptions the volumetric flow rate into the source chamber is much lower than the rate of outflow through the feeder-dyke (e.g., Stasiuk et al., 1993; Woods and Hubbert, 2003).

From these considerations it follows that the excess pressure as a function of time, *p(t)*, in the source chamber of the feeder-dyke at any instant is given by:

$$p(t) = p_e - \psi \int_0^t Q dt \tag{18}$$

where p_e is the excess pressure at the time of chamber rupture and feeder-dyke initiation, that is, at $t = 0$, and Q is the volumetric flow rate up through the feeder. Here ψ (with the unit of Pa m^{-3}) is given (cf. Eq. 20) by:

$$\psi = \frac{1}{(\beta_m + \beta_r)V_t} = \frac{p_e}{V_{er}} \tag{19}$$

where, as before, V_{er} is the volume of eruptive (including feeder-dyke) materials. The volumetric flow rate Q through the volcanic fissure (fed by a dyke), that is, the effusion rate, changes with time according to the equation (Machado, 1974):

$$Q(t) = Q_i - C \int_0^t Q dt \tag{20}$$

where Q_i is the initial volumetric flow rate and C is a constant that depends on the excess pressure, compressibility and volume of the magma chamber, and the dimensions of the feeder-dyke. Eq. (20) has the solution (Machado, 1974; cf. Wadge, 1981):

$$Q = Q_i e^{-Ct} \tag{21}$$

which shows that the volumetric flow rate out of the chamber (through the feeder-dyke) declines exponentially with time from the instant of magma-chamber rupture and feeder-dyke injection (and subsequent eruption) until the end of the eruption. A roughly exponential decrease in the volumetric flow or effusion rates is common during eruptions (Machado, 1974; Wadge, 1981; Stasiuk et al., 1993; Thordarson and Self, 1993; Thordarson and Larsen, 2007; Neri et al., 2011). One such example (with irregularities, however) is provided in Fig. 11.

Using similar arguments, it can be shown, based on the above assumptions and by analogy with Eq. (21), that the excess-pressure $p(t)$ in the magma chamber during the eruption is also a negative exponential function of time and given by:

$$p(t) = p_e \left(1 - e^{-(\frac{V_{er}}{Qt} - 1)} \right) \tag{22}$$

where Qt is the magma volume (in m^3) that flows out of the chamber/reservoir during the time interval t. The exponent has the units of m^3/m^3 and is thus dimensionless. Eq. (22) indicates an exponential decrease in excess pressure in the source chamber during the eruption until the excess pressure approaches zero, that is, $p(t) \to 0$, the bottom of the feeder-dyke closes, and the eruption comes to an end (Fig. 11). For eruption forecasting, one of the

main points is therefore to understand and estimate how long time will it take for $p(t) \to 0$, that is, for the eruption to end.

As an example, consider a moderate eruption of eruptive and intrusive volume V_{er} = 2 km^3 and take the excess pressure in the chamber, p_e, before rupture and dyke injection as the typical tensile strength of 4 MPa. We assume that the eruption comes to an end when $p(t) \to 0$. Furthermore, we also assume that there is negligible inflow of new magma into the chamber in comparison with the rate of outflow of magma during the eruption. While the peak eruption rate may be thousands of cubic metres per second, the average rate in many moderate eruptions is of the order of a few hundred cubic metres per second, or less. If we use the common value of Q = 100 m^{3}s^{-1}, then Eq. (22) gives the duration of the eruption as 2 × 10^{7}s or 33 weeks. An eruption of 33 weeks, or close to 8 months, is much longer than the median duration of eruptions, which is 7 weeks, based on data on 3301 eruptions compiled by Simkin and Siebert (2000). It is, however, very similar to the duration of the 2014-2015 eruption of Bardarbunga-Holuhraun in Iceland (Browning and Gudmundsson, 2015a).

The time for an eruption to come to an end as well as the total eruptive volume V_{er} leaving the chamber in that time (that is, Qt) depend on several factors but primarily on the total volume of the magma chamber (Eqs. 2-5). We have indicated above that reasonably large eruptions may need a special mechanism, that is, a mechanism different from the ordinary mechanism discussed above. Again, the exact eruptive volume for which such a special mechanism would be needed cannot be specified because it depends on the size of the source magma chamber or reservoir. However, it is known that all explosive eruptions exceeding about 25 km^3 of eruptive materials are associated with collapse calderas (e.g., Lipman, 1984, 1997). Furthermore, most, perhaps all, large effusive eruptions in rift zones are associated with grabens, commonly large ones. It is often argued that collapse calderas, and perhaps grabens, are the consequence of large eruptions. Here we shall explore the other possibility, namely that large eruptions are the consequences of caldera collapses and graben subsidences.

6. Mechanics of large eruptions

For generating large eruptions, we discuss here a new mechanism, based on gradual reduction in the chamber or reservoir volume during the eruption so as to maintain the excess pressure. This implies that the exponential decrease in excess pressure, as indicated by Eq. (22), is delayed until very late in the eruption. Here we first derive the model for large explosive eruptions, and take the piston-like caldera collapse as a driving force for maintaining the excess pressure in the chamber, hence for generating the large eruption. Following this, we turn to large effusive eruptions where, we suggest, grabens commonly play an analogous role to collapse calderas.

a. Large explosive eruptions

No really large eruptions have been recorded instrumentally. The largest explosive caldera eruption in the 20th century was the 1912 Novarupta eruption in Alaska (Wood and Kienle, 1992; Hildreth and Fierstein, 2012). This eruption produced some 30 km^3 of acid to intermedia tephra, calculated as equivalent to about 13 km^3 of magma leaving the magma

chamber. The part of the chamber that generated the caldera collapse during the eruption, however, is beneath the nearby volcano Katmai. The caldera is 3-4 km in diameter and 0.6 km deep, and with a volume of 5-6 km^3, so that its volume is much less than that of the magma volume leaving the chamber, as is commonly the case. Associated with the eruption were 14 earthquakes exceeding M6. The magma came partly from the chamber, or part of the chamber (possibly the same chamber is beneath Katmai and Novarupta), beneath Katmai, which is at about 10 km lateral distance from Novarupta. The chamber was layered with the acid (rhyolite) on the top and less evolved andesite at the bottom. Layering of a similar kind is common in magma chambers and reservoirs (cf. Fig. 9).

The second, and much better documented, explosive caldera eruption in the 20^{th} century was the 1991 Pinatubo eruption in the Philippines (Newhall et al., 1997). The eruption produced an estimated 10 km^3 of erupted materials, equivalent to about 4 km^3 of magma leaving the chamber, while some estimates suggest 5.3 km^3 (Stix and Kobayashi, 2008). The eruption was thus moderate in terms of volume. It was preceded by earthquakes—possibly as long as 8 months before the eruption, when a M7.8 earthquake occurred within 100 km of Pinatubo—and there were also earthquakes during the eruption. The associated collapse produced a caldera about 2.5 km in diameter.

Other medium to large explosive eruptions in the past centuries include the 1815 Tambora eruption in Indonesia (Self et al., 1984; Rosi et al., 1999). The estimated volume of eruptive materials (mainly ash) is 160-170 km^3, which is regarded as roughly equivalent to about 50 km^3 of magma leaving the chamber, making it probably the largest eruption in historical time. A large caldera, 6-7 km in diameter and with a maximum depth of 1200 m, was generated during the eruption (Self et al., 1984; Stothers, 1984). Self et al. (1984) estimate the caldera volume at 36 km^3, again smaller than the volume of eruptive materials. There was an unrest period with earthquakes for at least 3 years prior to the eruption.

The largest instrumentally recorded and historical explosive eruptions, however, are orders of magnitudes smaller than the largest known explosive eruptions (Pyle, 2000; Mason et al., 2004; Crosweller et al., 2012). The latter produced from many hundreds to several thousand cubic kilometres of eruptive materials. The most recent very large explosive eruption is the Toba eruption in Sumatra, some 74,000 years ago, which produced around 2,800 km^3 of eruptive materials (Chesner, 2012). Other eruptions on that scale include the La Garita Caldera eruption in Colorado (the United Stated), which generated the Fish Canyon Tuff some 27-28 million years ago, with an estimated volume of 4000-5000 km^3 (Lipman, 1997; Mason et al., 2004). The associated caldera itself is elongated with major and minor axes of 75 km and 35 km, respectively.

For explosive eruptions that happened long before historical time, as long as tens of millions of years ago or more, estimates of the volume of eruptive materials will always be inaccurate. Part of the material in such eruptions presumably falls on the sea or lakes, is carried away by erosion, buried by later eruptions, or affected in other way that make accurate area (and therefore volume) estimates impossible. However, the volumes given for these old pyroclastic rocks, such as those associated with the Toba eruption and the La Garita eruption (the Fish Canyon Tuff), refer to the estimated ‘dry-rock-equivalent’ volumes (Mason et al., 2004), which are similar in density to their source magmas. Thus, these volumes are a

crude measure of the actual minimum magma volume that left the source chamber during the eruption.

Explosive eruptions that start as 'ordinary' may develop into large eruptions in connection with caldera collapse. In most reasonably well-documented caldera-collapse eruptions, the eruption intensity, that is, the volumetric flow rate, reaches its peak at a later stage than in 'ordinary' eruptions. Ordinary explosive eruptions (and effusive eruptions as well) usually peak very quickly - some 42% (of 252 documented explosive historical eruptions) within the first day, and 52% within the first week (Simkin and Siebert, 2000). By contrast, some of the largest historical caldera eruptions reached their peak intensity only after many months, and some after many years. Here I suggest that for many large explosive eruptions the late peak or plateau in the eruption is partly attributable to the maintenance of the excess pressure and the development or reactivation of the caldera ring fault.

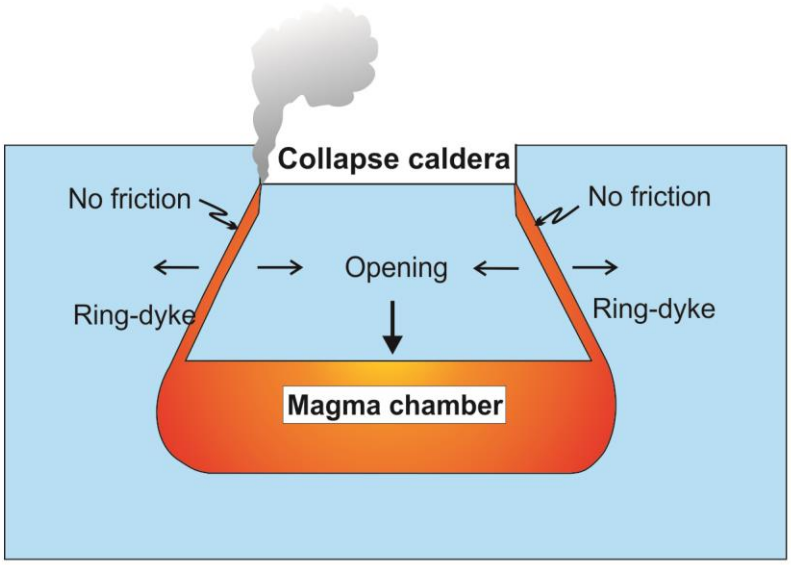

Fig. 12. *When caldera subsidence (vertical arrow) occurs on an outward-dipping (reverse) ring-fault, the ring-fault opening gradually increases as the subsidence progresses (as indicated by the horizontal arrows). Consequently, the ring-fault would normally be injected by a ring-dyke, and as the opening increases the dyke is likely to reach the surface and feed an eruption. While the ring-dyke is fluid, as it is normally during the entire collapse, there is essentially no friction along the ring-fault and the caldera block may subside to the bottom of a totally fluid chamber. This is referred to as unstable caldera displacement (Gudmundsson, 2015). It follows that (1) the volumetric flow or effusion rate should increase greatly with as the subsidence of the caldera block progresses, and (2) most (or all) of the magma in the chamber may be squeezed out during the eruption. A typical chamber with volumes of hundreds of cubic kilometres may thus produce an eruption of equal volume, that is, a very large eruption.*

Of the instrumentally monitored eruptions discussed above, in the both the explosive ones, namely the 1912 Novarupta eruption and the 1991 Pinatubo eruption, a large part of the caldera collapse occurred during or after the middle period of the eruption (Stix and Kobayashi, 2008). The details of the 1912 Novarupta eruption and the associated Katmai caldera collapse are of course poorly known, with very little seismic instrumentation on site and very poor seismic network in the world as a whole at that time. Nevertheless, the seismic

energy release or transformation appears to have increased in the second half of the eruption duration. Similar results, but much better documented, were obtained during the 1991 Pinatubo eruption, indicating that large part of the ring-fault displacement may have occurred during the middle part of the eruption duration. By contrast, in the three well-documented non-explosive caldera eruptions, that is, the 1968 Fernandina (Galapagos) eruption, the 2000 Miyakejima eruption, and the 2007 Piton de la Fournaise (Reunion) eruption - all of which were small - the ring-fault displacement continued in small steeps during the eruption, so that the seismic energy transformation was essentially constant for the main period of the collapse (Kumagai et al., 2001; Geshi et al., 2002; Stix and Kobayahsi, 2008; Michon et al., 2011; Fontaine et al., 2014).

These conclusions all rest partly on the results of analyses of the seismic energy released or transformed as a function of time during the collapse and associated eruption. For the Novarupta/Katmai event, the seismic data is really all there is because no scientists observed or monitored the event itself. The 1968 collapse of Fernandina was also before the time of high-quality GPS and InSAR geodetic studies, so that, again, the main information about the ring-fault displacement is through earthquake monitoring (Filson et al., 1973). While the conclusion that the different style of ring-fault slips between the explosive and non-explosive eruptions is reflected in the associated earthquake-energy release is plausible, there are several possible mechanical reasons for this difference in behavior. Among the main factors affecting ring-fault slip is the attitude of the fault and the related effect of possible ring-dyke formation.

There are two primary models on the attitude of the ring-faults of collapse calderas, and their differences have important implications for caldera eruptions. One model assumes that the caldera faults are outward dipping (Fig. 12), the other that the faults are inward dipping (Fig. 13). The outward-dipping model is well established in the caldera literature, and is the original idea—dating back to Anderson's (1936) model on ring-fault formation. This ring-fault attitude is also suggested by many analogue experiments (Marti et al., 1994, 2008; Acocella, 2007; Geyer and Marti, 2014). Most observed well-exposed ring-faults, however, seem to be close to vertical or steeply inward dipping (e.g., Simkin and Howard, 1970; Macdonald, 1972; Filson et al., 1973; Fedotov et al., 1980; Aramaki, 1984; Lipman, 1984; Newhall and Dzurisin, 1988; Lipman, 1997; Gudmundsson, 1998; Geshi et al., 2002; Browning and Gudmundsson, 2015b). Yet, there is some field evidence for outward-dipping ring-faults (e.g., Williams et al., 1970; Branney, 1995; Cole et al., 2005; cf. Geyer and Marti, 2008; Marti et al. 2009). Many ring-faults are occupied by ring-dykes, many of which are vertical or dip steeply inward (Oftedahl, 1953; Almond, 1977), while some may be outward-dipping (Anderson, 1936).

The outward-dipping model has several important implications for the course of the caldera-forming eruption, all of which relate to the gradual increase in the opening or

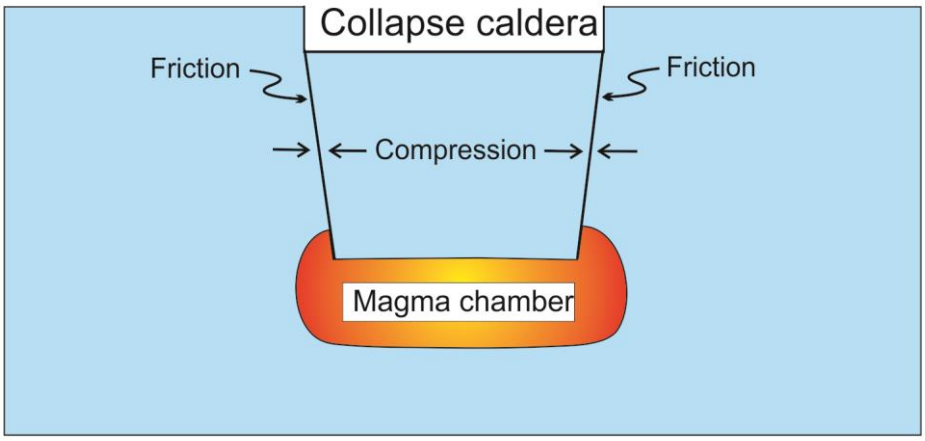

Fig. 13. *As a caldera block subsides on an inward-dipping normal ring-fault, the block becomes subject to gradually higher horizontal compression (compressive stress). So long as no ring-dyke is injected along the ring-fault, the friction together with the normal stress on the fault plane ensure that the fault remains closed and the caldera displacement stable (Gudmundsson, 2015). It follows that collapse on an inward-dipping normal ring-fault is less likely than collapse on an outward-dipping ring-fault to result in increasing volumetric flow or effusion rate through a ring-dyke as the subsidence increases (cf. Eq. 1). The normal-fault collapse is also unlikely to destroy the magma chamber.*

aperture of the ring-fault (the 'gap' between the piston-like caldera block and the walls of the host rock) as the caldera subsidence increases (Fig. 12). The implications are:

1. A ring-dyke must form and act as a feeder to a part of the eruption. This follows because there is no way that such an opening, which reaches all the way to the surface, could be connected to the magma chamber and not be injected by magma.
2. The volumetric flow rate through the ring-dyke should increase with increasing subsidence of the caldera floor. As the piston-like caldera block subsides into the magma chamber the opening between the host rock and the block gradually increases so that the aperture Δu in Eq. (1) increases. And since the volumetric flow rate through the feeder ring-dyke depends on Δu^3, that is, the aperture in the third power, the aperture increase with caldera subsidence should result in a great increase in the volumetric flow rate Q during the eruption so long as the caldera is subsiding.
3. Since there is essentially no friction (only that related to the magma viscosity of the ring-dyke) and increasing ring-fracture opening with increasing caldera subsidence, there is nothing to stop the piston-like block from sinking to the bottom of the chamber. This means that for an outward-dipping ring fault, essentially the entire magma chamber could erupt so that little magma would be left in the chamber following the collapse.

The data available today provide only partial tests of these three implications. Briefly, the present data indicate as follows. As to the first point, many calderas, for example in Iceland, have very thin or non-existing ring-dykes (e.g., Gautneb et al., 1989; Browning and Gudmundsson, 2015b). As to the second point, it is not clear if the volumetric flow rate increases as the caldera subsidence continues, or if the caldera eruptions are primarily related to ring-dykes. In some cases the eruption is partly along a ring-dyke, in others the eruption

appears to be primarily in the central part—from the main conduit of the stratovolcano that subsequently collapses or from a central part of an already existing caldera. Of the five main documented caldera collapses during the past 100 years or so, there was no ring-dyke eruption in at least four, namely: Novarupta-Katmai, Alaska (1912), Fernandiana, Galapagos (1968), Miyakejima, Japan (2000), and Piton de la Fournaise, Reunion (2007). If we include the 1975-1976 collapse of the Plosky-Tolbachik pit crater as the sixth caldera collapse then there was also no ring-dyke eruption during its collapse (Fedotov et al., 1980). Part of the eruption during the collapse in Pinatubo, the Philippines (1991), may have been on a ring-dyke, but the documentation indicates that much, perhaps most, of the eruption was along the central conduit (Stix and Kobayashi, 2008).

As for the Plosky Tolbachik volcano, it is a basaltic edifice (a shield volcano), and part of its summit collapsed during the 1975-1976 fissure eruption (Fedotov et al., 1980). The collapse, however, was associated with an existing pit crater. Also, the diameter of the floor of collapse was only about 700 m (Fedotov et al., 1980), and thus less than the minimum diameter of a typical caldera (often regarded as about 1 km). The maximum diameter at the rims (upper edge of the caldera), however, appears to have reached about 1300 m, in which case the collapse may be regarded as that of a caldera with a rather gently inward-dipping ring-fault.

As to the third point, some magma chambers are apparently destroyed by the caldera collapse. This follows since there is very little if any activity at the location of the caldera subsequent to its formation (e.g., Marti and Gudmundsson, 2000). Most calderas, however, are highly active after collapse (Newhall and Dzurisin, 1988), suggesting that the magma chamber is not destroyed during the collapse. As for the recent examples discussed above, there have been eruptions in Fernandina, Plosky-Tolbachik, Pinatubo, Miyakejima, and Piton de la Fournaise since their recent collapses, showing that the associated magma chambers are still there and active.

As for the inward-dipping model of collapse calderas (Fig. 13), the requirement for slip is extension across the ring fault. This extension can be generated either through cm-scale doming related to pressure increase in the deeper reservoir (Fig. 2), rift-related extension, gravity sliding resulting in volcano spreading, or any other similar mechanism that can produce extension (e.g., Gudmundsson, 2007). Because of the existing cavity-like shallow magma chamber, and particularly when the ring-fault starts do develop (or an existing one to slip), there will be tensile and shear stress concentration in and around the piston-like caldera block. The ring-fault development and subsidence of the piston-like block is also likely to generate further inflation. This follows for two reasons (Gudmundsson, 1998, 1999). (1) The subsidence of the caldera block reduces the effective thickness of the crustal plate or segment above the deeper source reservoir which contains the magma chamber and the caldera (Figs. 9, 13, and 14). The reduction in the effective thickness diminishes the flexural rigidity of the plate, so that for a constant or even reduced magmatic excess pressure in the reservoir, the plate (and thus the caldera) becomes subject to further upward deflection or doming. (2) For an inward-dipping (normal-fault) caldera the footwalls (the flanks) rise as the caldera-block subsides, as is the rule for normal faults, particularly those extending down into magma chambers and reservoirs (Gudmundsson, 1998). Thus, while the magma under the subsiding caldera-block becomes subjected to increased or constant pressure during each ring-fault slip,

the magma located below a rising footwall is subject to reduced vertical stress. It follows that there may be explosive gas expansion of (particularly felsic) magma in the part of the chamber that is beneath the ring-fault footwall, thereby maintaining a high excess pressure. This excess pressure can be maintained for a while through repeated ring-fault slips, thereby contributing to squeezing out large fraction of the magma in the chamber and, because of the location of the excess-pressure maintenance, possibly contributing to the formation of a ring-dyke. The ring-dyke, in turn, helps overcome the friction and promotes caldera subsidence.

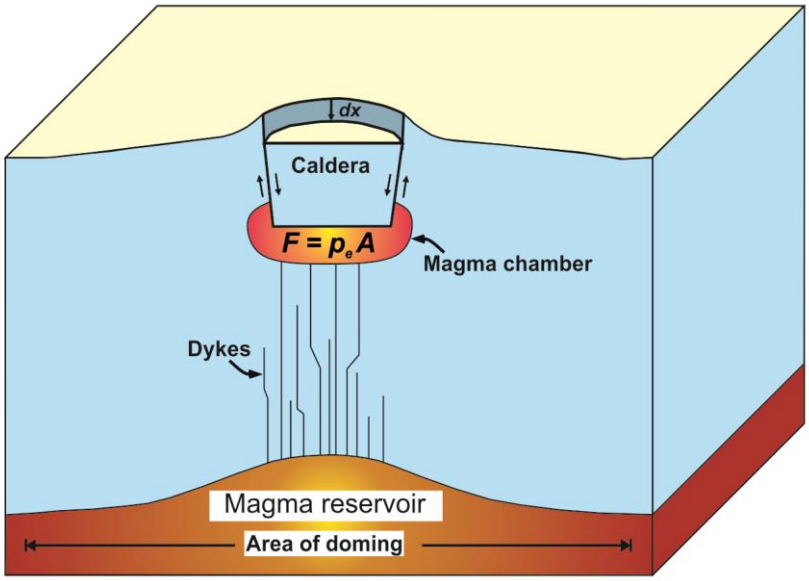

Fig. 14. *When a caldera block subsides – here denoted by the differential distance dx - into the associated shallow magma chamber, the volume of the chamber is reduced (the chamber shrinks). It follows that the excess pressure in the chamber is roughly maintained, thereby allowing much larger fraction of the magma to be squeezed out of the chamber than during an ordinary poroelastic eruption. The excess pressure* p_e *is related to the average force on the cross-sectional area of the subsiding caldera block A through* $F = p_e A$ *(Eq. 23). Commonly, the formation or reactivation of a collapse caldera is either due to an extension or a small uplift or doming of the crustal segment hosting the potential or existing caldera.*

For a (close to) vertical ring fault and/or ring dyke injection (Fig. 5) there may be a total collapse, in which case the magma chamber is to a large degree emptied. For other conditions, the friction on an inward-dipping ring-fault (Fig. 13) limits the subsidence to a normal maximum of 1-2 km. Also, where the friction is highest, for example on parts where there is no ring-dyke or the dip of the ring-fault is unusually gentle, there may be little or no slip during the collapse, thereby generating trap-door calderas (Amelung et al., 2000). Thus, for inward-dipping ring-faults, the slips are more controlled than in the case of outward-dipping faults. Both cases, however, reduce the volume of the magma chamber, thereby offering the possibility of maintaining the excess pressure at high or close to constant level for a longer time and squeezing out unusually large fraction of the magma in the chamber. Such an excess pressure maintenance implies that the exponential decrease in the magma-chamber excess pressure (Eq. 22) occurs only comparatively late in the eruption. For inward-

dipping ring fault, the excess pressure may also be maintained through rise of the ring-fault footwalls during repeated slips. These processes offer a possible mechanism of generating large eruptions—eruptions of many tens or hundreds of cubic kilometers from typical-sized chambers, the latter being in excess of 5 km^3 (except at some fast-spreading mid-ocean ridges, where they may be smaller) and normally in the range of 20-500 km^3.

6.2 Energy of caldera eruptions

For analysing the excess-pressure effect of piston-like caldera-block subsidence into a shallow chamber, consider the magma chamber in Fig. (14). Excess pressure times the cross-sectional area of the caldera *A* is the force *F*, that is:

$$F = p_e A \tag{23}$$

As the piston-like caldera roof moves the differential distance *dx* (Fig. 14), the corresponding very small (infinitesimal) work *dW* done by the surroundings on the magma chamber system (Fig. 2) is:

$$dW = Fdx = p_e A dx \tag{24}$$

and the volume of the chamber changes by dV_c , that is:

$$-dV_c = Adx \tag{25}$$

The minus sign in Eq. (25) is to indicate that chamber volume decreases during the piston-like caldera subsidence. Here we follow the thermodynamic convention that work done on the system is regarded as positive. Combining Eqs. (24) and (25), and using the relation $dW = dU$ (the first law of thermodynamics when no heat is added to the system), where *dU* is the change in internal energy of the magma chamber during its shrinkage or contraction, we get:

$$dU = -p_e dV_c \tag{26}$$

which is a measure of the elastic potential energy *dU* transformed during an caldera eruption as a function of the excess pressure p_e and the contraction or shrinkage of the chamber dV_c.

As indicated above, the excess pressure p_e at the time of magma chamber rupture and feeder-dyke injection is roughly equal to the in situ tensile strength, T_0 (Eq. 16). The tensile strength, in turn, is almost a constant, mostly 2-6 MPa and typically around 4 MPa. It follows that the excess pressure p_e at the time of chamber rupture is essentially constant, here about 4 MPa, and in the present model this pressure is maintained until close to the end of the caldera-forming eruption, at which stage exponential pressure decline sets in (Eq. 22). It then follows from Eq. (26) that the elastic potential energy of the eruption is directly related to the contraction or shrinkage of the chamber during the eruption, that is, dV_c, which corresponds roughly to the volume of material the leaves the chamber during the eruption. Feeder-dyke

volumes are normally fraction of a cubic kilometer, and maximum several cubic kilometers. For large eruptions (tens or hundreds of cubic kilometers or more) the feeder-dyke volume may be regarded as included in the estimated (and uncertain) eruptive volume V_{er}.

From these considerations it follows that we can identify V_{er} with $-dV_c$ to obtain the elastic potential energy U_{er} driving the caldera-forming eruption from the following equation:

$$U_{er} = p_e V_{er} \tag{27}$$

From Eq. (27) the elastic energy driving an explosive eruption of a given volume can be estimated, as we shall do below. First, however, we shall extend this analysis to large effusive eruptions.

6.3 Large effusive eruptions

The volumes of numerous basaltic lava flows reach many tens and hundreds of cubic kilometres, and some reach thousands of cubic kilometres. Eq. (17) indicates that there are limits to how large lava flows can be generated in a single eruption by the ordinary

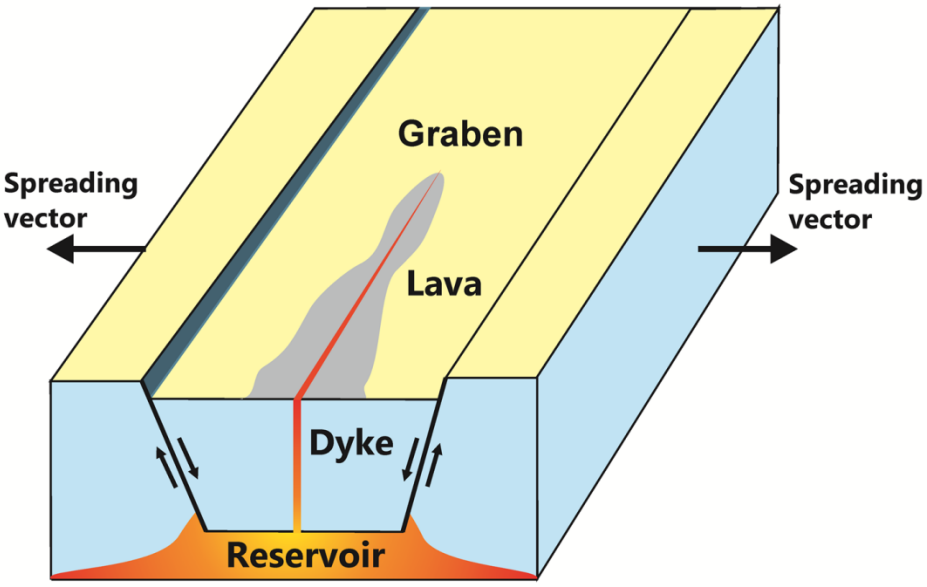

Fig. 15. *Subsidence of a graben block within an active volcanic zone or system during an eruption reduces the volume of the associated reservoir. The resulting reduction in reservoir volume, if rapid enough, may largely maintain the excess pressure in the reservoir. It follows that a much higher proportion of the magma can be squeezed out of the reservoir during the eruption than would be possible in ordinary eruptions in the absence of rapid graben subsidence.*

mechanism. For example, a lava flow of 100 km^3 would, according to Eq. (17), require a reservoir with a volume of 5×10^5 km^3. To reach such a volume the reservoir that was as long as 1000 km and as wide as 20 km wide, would have to be 25 km thick. A magma body of these dimensions is perhaps not very likely to exist at any particular time and location to supply magma to a single eruption. Even effusive eruptions that reach tens of cubic kilometres would seem to require unusually large reservoirs or a different mechanism. And

the largest effusive eruptions, such as the comparatively recent (16-17 million year-old) Columbia River basalts, reach volumes of as much as several thousand cubic kilometres (Reidel et al., 1989; Tolan et al., 1989; Hooper et al., 2007). It is extremely unlikely that such volumes could be generated by the ordinary mechanism that results in the ratio given by Eq. (17).

Here I propose a new mechanism for generating large effusive eruptions, in particular basaltic lava flows with volumes from tens up to thousands of cubic kilometers. This mechanism is basically similar to the one for generating large explosive eruptions, namely subsidence of a crustal block into the reservoir during the eruption (Fig. 15), thereby maintaining the excess pressure and greatly increasing the V_{er}/V_b ratio (Eq. 17). As the crustal segment within the graben subsides, it maintains the excess pressure (and may occasionally increase the pressure during the subsidence process) in the reservoir (or, for a shallow graben, magma chamber) below in a manner outlined for the collapse calderas above (Eqs. 23-26).

Fig. 16. *Aerial view of the Thingvellir Graben, of Holocene age (here snow-covered in the winter). View northeast, the graben is about 5 km wide where the two main boundary faults enter Lake Thingvallavatn (dark blue). The lava shield Skjaldbreidur (Fig. 10) is seen in the northeast.*

While the mechanism is quite general, some specific examples may be discussed. The postglacial Skjaldbreidur lava shield in Iceland (Figs. 10 and 16) has estimated volumes ranging from 13.5 km^3 (Sinton et al, 2005) to 17 km^3 (Saemundsson, 1992), with an average estimate of about 15 km^3 (Rossi, 1996). The exact age of Skaldbreidur is not known, but based on mapping it is in the range of 6000-9000 B.P., and probably closer to 9000 B.P. (Sinton et al., 2005). The northern part of the largest postglacial graben in Iceland, the

Thingvellir Graben (Figs. 7 and 16), is mostly located in an older lava flow, a pahoehoe flow referred to as the Thingvallahraun (Thingvellir Lava). It had previously been estimated to have formed at about 10,200 B.P. (Sinton et al., 2005), and thus perhaps as much as 1000 years before the Skjaldbreidur shield.

There are indications that much of the faulting and tension-fracture formation in many fissure swarms in Iceland occurred in early postglacial time (Gudmundsson, 1986, 1987a,b). This is, to a degree, supported by recent GPS measurements which suggest that the current rate of extension in the entire West Volcanic Zone, including the Thingvellir Graben, is considerably less than the average dilation of about 10 mm/year since the Holocene lava flow Thingvallahraun was formed (Arnadottir et al., 2008). It is also supported by the lava shield itself being basically unfaulted and by general considerations of the tectonic evolution of the Thingvellir Graben (Sonnette et al., 2010). Thus, no large normal faults and tension fractures dissect the main shield itself (Figs. 10 and 16), and this part of the West Volcanic Zone (Fig. 7) is essentially free of tectonic fractures. Thus, tens of meters of subsidence along the Thingvellir Graben may have occurred in early Holocene. The graben extends into the lake (Fig. 16) and south to the Hengill Volcano (Fig. 7). There the boundary faults dissect Pleistocene rocks, some of which have displacements exceeding 200 m (Saemundsson, 1992). The extension of the Thingvellir Graben to the south, through Lake Thingvallavatn and to the Hengill Volcano, is likely to have active during early Holocene at the same time as much of the Thingvellir graben itself formed. To the west, the graben structure extends to normal faults in Pleistocene rocks where the displacements reach about 400 m. It is not known if these faults participated in the postglacial subsidence. It is well known that part of the displacement on a normal fault is due to rise of its flanks, but the greater part is normally related to absolute subsidence.

If the extended Thingvellir Graben is taken as 50 km long and 7 km wide (Figs. 7 and 16; Gudmundsson, 1987b), then its area is about 350 km^2. An overall subsidence of 30-40 m for the extended graben as a whole corresponds to a volume of 10-14 km^3, which is roughly the volume of the Skjaldbreidur lava shield. If the entire graben system of the West Volcanic Zone was involved, in which case Skjaldbreidur is roughly in the centre (Figs. 7 and 16), then the total length is about 85 km and the total width about 18 km, in which case the area is about 1500 km^2. For such a graben system, a subsidence of mere 10 m would be sufficient to correspond to the entire volume of Skjaldbreidur, 15 km^3. For such a simple analysis, several factors must, however, be considered, namely:

- Part of the subsidence of the graben must be younger than the formation of the Skjaldbreidur shield and thus cannot have contributed to the maintenance of the excess pressure in the reservoir. This follows because displacement occurred in 1789 AD and presumably earlier. However, there is general agreement that a large fraction of the subsidence along the faults occurred in early Holocene (Gudmundsson, 1987b; Sonnette et al., 2010).
- The maximum displacement on the Holocene faults is about 40 m, so that a general displacement of 30-40 m may look like an overestimate. However, the faults continue into Lake Thingvallavatn (Fig. 16; Bull et al., 2003) and south to the volcano Hengill (Fig. 7) where they reach displacements of at least 200 m. It is not known how large fraction of the 200 m displacement was generated during the formation of the

Skjaldbreidur lava shield, but it may be in excess of 40 m. Furthermore, the total subsidence of the Thingvellir Graben may be much larger; Tryggvason (1982) estimates the maximum Holocene subsidence in the graben as 70 m.

- The eruption possibly took many decades. The volumetric flow rates are of course not known, but by analogy with other eruptions, Sinton et al. (2005) speculate that the eruption may have taken 40-80 years. If true, then inflow into the reservoir could also contribute to maintain its excess pressure during the eruption.

Large grabens are normally associated with flood basalt provinces or traps. There are, for example, very large grabens in the Columbia River Plateau, including the Oregon-Idaho Graben. This particular graben is 50-60 km wide and 100 km long (Cummings et al., 2000), and thus with an area of at least 5000-6000 km^2. With maximum graben subsidence of as much as 800 m, there is a clear potential for squeezing out magma during the graben development that reaches the volumes of the large Columbia River lava flows. Indeed, the authors of this particular study of the Oregon-Idaho Graben conclude that its formation coincided with large eruptions, but consider that the flows were primarily of rhyolite and that the graben itself (of age 15.3-15.5 Ma) developed after the main basaltic lava flows of the Columbia River formed (Cummings et al., 2000). Further studies on the volcanotectonic relationship between grabens and flood basalts are clearly needed. In particular, since, in terms of the model proposed here, subsidences of grabens of sizes similar size would be candidates for squeezing out large volumes of magma from deep-seated reservoirs, such as occurs during flood-basalt eruptions.

7. Elastic energy release in large eruptions

Equations (26 and 27) have several implications for quantifying large eruptions. First, if we rewrite Eqs. (26) and (27) in the forms:

$$p_e = -\frac{dU}{dV_c} \tag{28}$$

and

$$p_e = \frac{U_{er}}{V_{er}} \tag{29}$$

we see that the magmatic excess pressure may be viewed as energy per unit volume or as energy density. This interpretation, however, assumes that no heat is added to the system during an eruption. Within the framework of thermodynamics, this means that the first law, given in terms of very small (infinitesimal) changes in heat dQ and work , dW, of a system, namely:

$$dU = dQ + dW \tag{30}$$

becomes (with $dQ = 0$):

$$dU = dW \tag{31}$$

where dU is infinitesimal change in the internal energy of the system. Here the system is the magma chamber, the reservoirs, and the hosting crustal segment (Fig. 2). Eq. (31) means that the change in internal energy dU equals the change in work dW done on the system. It should be noted that dQ and dW are path dependent and thus inexact differentials; that is, they are path (rather than state) functions, whereas dU is a state function and thus a proper or exact differential. The values of a state function are independent of its path from the initial to the final stage, and depend only on the state or conditions of the system. We do not denote dQ and dW by special symbols, as is sometimes done, since their path dependence is supposed to be known (cf. Sommerfeld, 1964).

The second implication is that, because pressure is analogous to stress, stress may be also interpreted as energy per unit volume or energy density. This implication can then be used for understanding better energy release rate during dyke and fault propagation and the associated material toughness, given as energy per unit volume or unit area. The energy release rate and material toughness both connect with the energy budget of volcanoes and volcanic zones/fields and also, in a different context, the energy budget of seismic zones (Gudmundsson, 2014).

The third implication relates to the contraction of the magma chamber; more specifically, that its shrinkage dVc corresponds roughly to the volume of material that leaves the chamber during an eruption. As indicated above, the volume that leaves the chamber includes not only the erupted material but also the intruded material, the latter being primarily the volume of the feeder-dyke. The feeder-dyke volume may be a large part of the volume that leaves the chamber for small to medium eruptions – and, of course, the entire part of unrest periods with dyke injections that do not result in eruptions. For eruptions of the order of hundreds of cubic kilometres or more, however, the feeder-dyke volume is normally insignificant. For example, a very long feeder-dyke would be 25-30 km, such as the 27-km-long feeder of the 1783 Laki eruption in Iceland (Fig. 7). A feeder-dyke with a strike dimension (length) of 27 km, dip dimension (height) of 20 km, and a thickness of 10 m—all dimensions similar to those estimated for the Laki feeder-dyke (Thordarson and Self, 1993)—would have a volume of about 5 km^3. While this is about 25% of the total volume leaving the reservoir that supplied magma to the Laki eruption (eruptive materials about 15 km^3 and dyke material about 5 km^3, based on this estimate), the dyke volume would be only 5% of a fissure eruption of 100 km^3, and proportionally less for larger eruptive volumes.

Typical collapse calderas on Earth are about 10 km in diameter, even if the largest ones reach 90-100 km (Gudmundsson, 2008). A ring-dyke injected along the entire ring-fault (Figs. 5 and 12) of circular caldera 10 km in diameter and with a source chamber (chamber roof) at 5 km depth would have an area of $A = 2\pi rh$ = 157 km^2. Some ring-dykes are up to hundreds of metres in thickness, but are then presumably formed in many injections (except, possibly, if injected along rapidly formed outward-dipping faults, Fig. 12). Many, and perhaps most, ring-dykes are of the order of metres or tens of metres in thickness. For the ring-dyke with the above area (using the assumed maximum depth of a shallow chamber, 5 km, as the source depth), the volume of a 10 m thick dyke would be about 1.6 km^3 and the volume of a 100 m thick dyke 16 km^3. Thus, even for a very thick ring-dyke, of the order of

100 m or more, and injected from comparatively great depth (for a shallow chamber), the ring-dyke volume is only a few percent (or less) of the volume of a very large explosive eruption of the order of hundreds or thousands of cubic kilometres. For such eruptions, as well as the similar-sized effusive eruptions discussed above, the feeder-dyke volume may be regarded as included in the total estimated eruptive volume (commonly with an uncertainty much larger than several cubic kilometers), as is done in the calculations below.

Consider first the very large explosive eruption of Toba in Sumatra, around 74,000 years ago, which produced some 2,800 km^3 of eruptive materials (Chesner et al., 1991; Chesner, 2012; Jaxybulatov et al., 2014). This is the estimated as solid-rock equivalent volume and includes the dyke material. Using the typical excess pressure of 5 MPa, Eq. (27) gives the elastic energy transformed during the eruption, by means of magma-chamber shrinkage, as 1.4×10^{19} J. The elastic energy is largely released thorough the shrinkage of the magma chamber, most of which was related to the associated caldera collapse (Figs. 5 and 15). We can thus also try to estimate the transformed elastic energy directly from the (crudely) estimated ring-fault size and displacement.

To do so we use basic results from fracture mechanics. A ring-fault has a free surface (a fluid surface) at its top (for example, the earth's atmosphere or a caldera lake) and its bottom (the magma in the associated chamber). In terms of fracture mechanics, the ring-fault is thus a through-crack and the type of displacement (movement of the fault walls) is mode III (Gudmundsson, 2011). The energy transformed or released U_{III} during ring-fault slip is, in terms of stress drop or driving shear stress $\tau_{d,}$ given by:

$$U_{III} = \frac{\tau_d^2 (1+\nu)\pi a A}{E} \tag{32}$$

where ν and E are Poisson's ratio and Young's modulus (stiffness) of the host rock, respectively, a is half the strike dimension or rupture length (half the perimeter) of the slipping ring-fault, and A is the total slip or rupture area (slip surface) during the ring-fault displacement. Most ring-fault displacements occur in many slip events, each associated with a driving shear stress and energy release. The cumulative energy release can then be estimated as the total energy transformed during all the slips (Stix and Kobayashi, 2008; Michon et al., 2011). For ring-fault slips, particularly those that happened long before instrumental recording and monitoring, it is often more convenient to use the total or cumulative (strictly the maximum) ring-fault displacement Δu_{III} during the collapse to estimate the energy transformed or released. Thus, in terms of total maximum ring-fault displacement the energy transformed is given by:

$$U_{III} = \frac{E \Delta u_{III}^2 \pi A}{16(1+\nu)a} \tag{33}$$

where all the symbols are as defined above.

Let us now calculate the cumulative or total energy released during the collapse associated with the Toba eruption 74,000 years ago. Lake Toba caldera is crudely elliptical in

plan view, with a semi-major axis of about 50 km and a semi-minor axis of about 15 km. The total area of the caldera is estimated at 2270 km^2 (Chesner, 2012); if modelled as a pure ellipse with the above semi-axes, the corresponding area would be about 2356 km^2. While the Toba caldera as a whole formed in several large eruptions, dating back to about 1.2 Ma (Chesner, 2012), the youngest large eruption, namely the one 74,000 years ago, formed most or all of the caldera seen today. The parameters in Eq. (33) may be estimated as follows. We assume a shallow magma chamber with a top at about 5 km depth. There are indications that at the present chamber may be somewhat deeper (Jaxybulatov et al., 2014), but it is likely that the chamber just before the collapse 74,000 years ago had expanded and had a roof that was shallower than today. From this and the perimeter of the caldera, we estimate the rupture (slip, collapse) area as roughly 1×10^9 m^2. Because caldera collapse (ring-fault displacement) may take from days to months or more (Stix and Kobayashi, 2008; Michon et al., 2011) and is thus generally very slow in comparison with the velocities of seismic waves, we use the static Young's modulus. For the uppermost 5 km of the crust in an active volcanic area, the average static Young's modulus is likely to be around 30 GPa (Gudmundsson, 2011), although it may be lower in highly fractured rocks, or rocks with many soft pyroclastic and/or sedimentary layers. Poisson's ratio is taken as 0.25, as is typical for most rocks.

The total vertical displacement during the collapse Δu_{III} is not well constrained. The elevation difference between the present bottom of Lake Toba and the caldera rim is from 900 m to 1700 m (Chesner, 2012). It does not follow, however, that the displacement was in this range, since the collapse 74,000 years ago partly followed existing earlier collapses. Also, there has been much deformation (resurgence) in the caldera since this last major collapse. If we use the caldera area, 2270 km^2, and assume that the displacement of the piston-like caldera block was such as to squeeze out 2800 km^3 of magma from the chamber, then the average vertical displacement on the ring-fault would be about 1230 m. It is known that caldera volumes are commonly different from the eruptive volumes, either larger or smaller. Nevertheless, in these crude estimates we take the vertical displacement at 1200 m. Using this value for the displacement, as well as the above estimates for Young's modulus, Poisson's ratio, and ring-fault area and perimeter, Eq. (33) yields U_{III} as about 6.8×10^{19} J. It follows that the ring-fault displacement elastic energy release is of the same order of magnitude as was obtained through direct calculation using the eruptive volume given by Eq. (27), that is, 1.4×10^{19}J.

As indicated above, the eruptive volumes of the largest explosive and effusive eruptions are both estimated at about 5000 km^3. Using Eq. (27) and the same excess pressure as above, 5 MPa, the elastic energy released during these eruptions is of the order of 3×10^{19} J. Thus, whether calculated based on the largest caldera collapses known on Earth, or based on the largest eruptive volumes known on Earth, the maximum elastic energy released or transformed in the eruptions is of the order of 10^{19} J. For comparison, the elastic energy release in the largest instrumentally measured earthquake ever recorded, the M9.5 Chile (Valdivia) earthquake, is of the same order of a magnitude, namely 10^{19} J, while the seismic moment is estimated at 10^{23} J (Gudmundsson, 2014). Thus, the largest volcanic eruptions and the largest earthquakes release or transform elastic energy of the same order of magnitude, namely 10^{19} J.

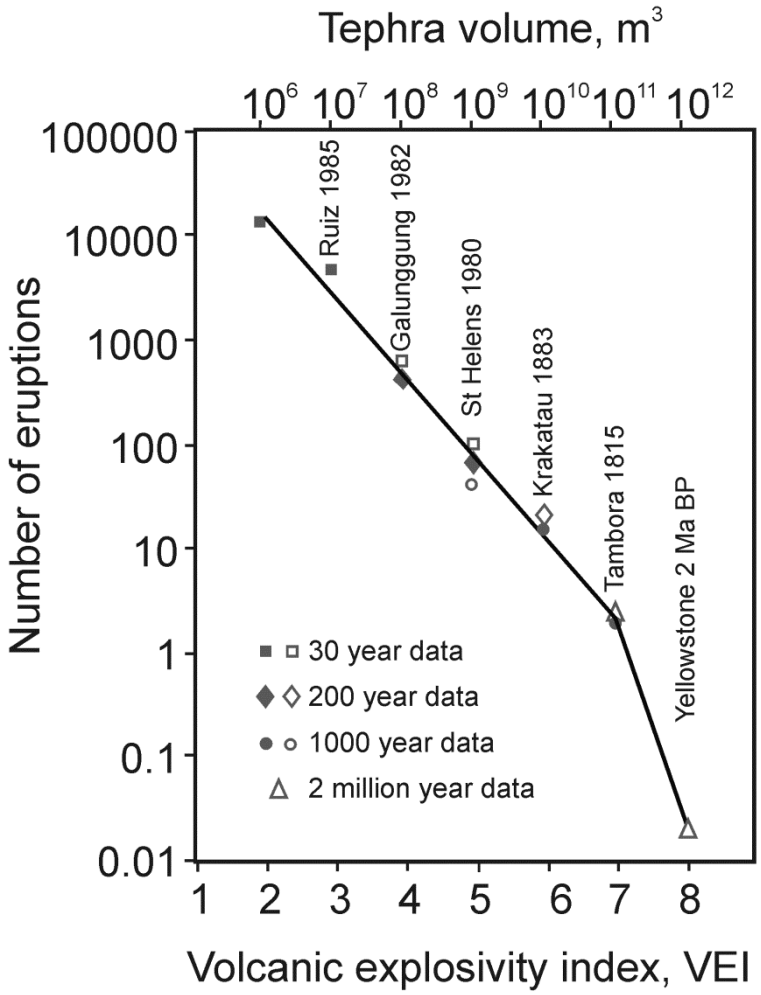

Fig. 17. *Number of eruptions in relation to their Volcanic Explosivity Index, VEI. The diagram shows the cumulative number of volcanic eruptions, for different intervals and normalised by 1000 years (that is, number of eruptions per 1000 years), for each VEI class. This bi-logarithmic plot has a clear break in the slope of the line (change in scaling exponent) at VEI magnitude 7, which is roughly where the eruptions become large in the present classification. Modified from Simkin and Siebert (2000).*

8. An elastic-energy magnitude scale for eruptions

How should we quantify eruptions, particularly large eruptions? For many years, this has been done using a magnitude scale referred to as the Volcanic Explosive Index (VEI), initially proposed by Newhall and Self (1982). Basically, the scale classifies the eruption explosivity through a combination of eruptive volume, height of eruption column (plume), and various qualitative assessments. The magnitude scale was especially designed to estimate the explosive magnitudes of historical eruptions, particularly through the amount of tephra produced and plume height (Tsuya, 1955; Hedervari, 1963; Mason et al., 2004; Crosweller et al., 2012), but has also been extended to pre-historic eruptions – in fact to eruptions that happened millions of years ago (Fig. 17). For the pre-historic eruptions, the assigned magnitude relies much on the estimated volume of tephra/pyroclastic material produced, whereas the plume height is of great importance when estimating the magnitudes of documented historical explosive eruptions (Pyle, 2000). Thousands of eruptions have been

classified based on the VEI. As the name implies, however, VEI is primarily a measure of the explosivity of an eruption, and relates only marginally to other quantitative measures of eruption sizes. For example, large effusive eruptions, being mostly non-explosive, normally do not score as high on the VEI scale as they would in case the eruptive volume was the main criteria (Pyle, 2000).

Another measure of eruption size is eruption intensity, given as eruption rate. More specifically, eruption intensity measures mass-eruption rate, which is the mass of eruptive materials produced per unit time, and has the unit kg s^{-1} (Fedotov, 1985; Carey and Sigurdsson, 1989; Pyle, 2000). Both the eruption intensity and the eruption magnitude, as measured through the VEI, are logarithmic, using the common logarithm.

The third measure of eruption size is the only one that relates directly to energy release. This is the thermal energy released or transformed during the eruption (e.g., Yokoyama, 1957; Pyle 1995, 2000). While the thermal energy released in an eruption may be several orders of magnitude larger than any other energy transformed during the eruption (e.g., Pyle, 2000; Smil, 2008), the cumulative thermal energy released in eruptions each year is a very small fraction of the thermal energy released through the worldwide geothermal flux. The annual cumulative thermal energy released in eruptions may be somewhere between 0.5% and 2% of the energy released through the general cooling of the Earth (Elder, 1976; Verhoogen, 1980).

During an eruption, the thermal energy released can mainly be attributed to the solidification and cooling of the erupted materials. Solidification of magma and the subsequent cooling of the volcanic rock to ambient temperatures is a continuous process; it operates in all active volcanic areas and, in particular, in and around magma chambers of individual polygenetic volcanoes. Thermal energy, however, is 'low-grade' energy in the sense that only a fraction of it can be transformed into other types of energy – including elastic energy, electric energy, and (mechanical) work. During eruptions, part of the thermal energy may be transformed into work for driving the upward movement of fine particles in buoyant volcanic plumes (Sparks et al., 1997; Mason et al., 2004). Thermal energy, however, has normally little, if any, role to play in magma-chamber rupture, feeder-dyke formation, and squeezing magma out of the chamber - namely the processes that lead to and maintain an eruption.

Equations (26) and (27) suggest a new measure of the size of a volcanic eruption, namely the elastic energy released or transformed during the eruption. As we have seen, such a measure can be compared directly with the energy released in earthquakes. Indeed, as mentioned, the elastic energy released in the largest eruptions is of the same order of magnitude as the energy released in the largest earthquakes (Gudmundsson, 2014). While further development of this measure could include the thermal energy associated with eruptions and earthquakes, changes in the potential energy of the magma, and other forms of energy transformation, the focus here is on the elastic energy release itself. More specifically, Eq. (27) can now be used as the basis of a new magnitude scale for volcanic eruptions.

Because the volume change or shrinkage of the chamber is a measure of the elastic energy transformed (Eq. 27), it follows that, for this magnitude scale, the volume (m^3) of the eruptive (plus intrusive) materials produced during an eruption should be used rather than the mass (kg) of the eruptive materials. The estimated eruptive volumes have of course an

uncertainty, particularly for eruptions that occurred millions of years ago. Yet, the uncertainty or error is normally within a factor of 2-3, so that the estimated volume may be regarded as of the correct order of a magnitude. And the order of magnitude of the elastic energy released in the eruption is normally all we need to know, and can hope to estimate, for large to great eruptions – which are of the greatest concern for mankind.

The general form of the proposed scale for elastic-energy magnitude M_e for volcanic eruptions is:

$$M_e = A\log U_{er} - B \tag{34}$$

Here, as above, U_{er} is the elastic potential energy of the eruption, log is the common logarithm (to the base of 10), and A and B are empirically determined constants. Once the constants have been determined from empirical data such as in Fig. (1), the magnitude scale can be fine-tuned and applied to all volcanic eruptions with estimated eruptive/intrusive volumes. This is important because for many pre-instrumental eruptions, that is, eruptions earlier than the past 100 years or so the only quantitative information available is (roughly) the volume of their erupted materials. For some caldera-driven eruptions, the caldera volumes are also known, and can be used, through Eq. (33), as an additional estimate of the elastic energy released in the eruption – as we did above for the Toba eruption which occurred 74,000 years ago. This eruption magnitude scale is thus directly connected to energy release and transformation and may be regarded as complementary to those that already exist.

9. Discussion

Very large eruptions are one of the greatest threats to the survival of mankind. The only other natural hazards of similar magnitudes are large meteoritic impacts. In the past 30 years, there has been considerable progress in understanding the mechanics of small to medium eruptions, that is, those that I refer to as 'ordinary' eruptions. Given the sizes of typical magma chambers, we know what sizes of ordinary eruptions they are capable of generating. These are mostly in the range of 10^{-2} km^3 to 10 km^3. While such eruptions can have large negative impact on their surroundings, including economic effects—such as the 2010 Eyjafjallajokull eruption in Iceland—they do not pose a hazard for the entire mankind. By contrast, very large eruptions—sometimes referred to as super-eruptions—pose a threat to the life and prosperity of humans as a species as well as many other animal species on Earth.

Large (and small) eruptions derive from magma chambers/reservoirs, whose formation and evolution has received much attention in the past decades. Research topics have included magma-chamber initiation, usually assumed to relate to accumulation of smaller intrusions (e.g., Gudmundsson, 1990; Burov et al., 2003; de Silva and Gosnold, 2007; Annen, 2011), stability and longevity (Kalstrom et al., 2010; Gelman et al., 2013; de Silva and Gregg, 2014), and the conditions for rupture or dyke injection (e.g. Fialko and Rubin, 1998; Folch and Marti, 1998; Gudmundsson, 2006; Grosfils, 2007; Gerbault et al., 2012). While there is a general agreement as to the basic mechanism of magma-chamber formation through multiple magma injections (intrusions), there are widely different views as to the conditions for magma-chamber rupture. These divergent views are discussed in detail by Gudmundsson

(2012). Here the conditions used are those of standard rock physics, whereby rupture occurs when the excess pressure in the chamber reaches the tensile strength of the host rock (Eq. 16). As indicated above, the tensile strength values used to assess these conditions, and for related aspects of the theory presented here, namely 0.5-9 MPa (with the typical value of 4 MPa), derive from in-situ measurements (cf. Gudmundsson, 2011).

Caldera formation and eruptions have also been widely discussed and analysed through field observations, as well as analogue, analytical, and numerical models (e.g., Burov and Giullou-Frottier, 1999; Floch and Marti, 2004; Hughes and Mahood, 2011; de Silva and Gregg, 2014). Particular attention has also been given to the relation between calderas and regional tectonics (e.g., Acocella, 2007; Holohan et al., 2008).

Given the importance of understanding the conditions for large eruptions, many studies have focused on the relation between collapse calderas and large eruptions (e.g., Roche and Druitt, 2001; Burov et al., 2003; Hughes and Mahood, 2011; Gregg et al., 2012; de Silva et al., 2014; Gregg et al., 2015), while others have provided more general considerations of large eruptions with, or without, associated caldera collapses (e.g., Lavallee et al., 2006; Costa et al., 2011; Caricchi et al., 2014). Nearly all these studies, however, focus on the mechanisms of large explosive eruptions, rather than effusive eruptions. Also, almost all the studies on caldera formation in relation to large eruptions use the underpressure model (discussed in detail below) as a basis. More specifically, it is assumed that large explosive eruptions generate underpressure in the associated magma chamber which, eventually, reaches a critical value at which caldera collapse occurs. The caldera collapse is then the consequence of the eruption, whereas in the present model the large explosive eruption is the consequence of the caldera collapse (Gudmundsson, 1998, 1999).

In contrast to the well-explored relation between calderas and large explosive eruptions, the potential relation between grabens and large (primarily) effusive eruptions has received little attention. In the present model, excess pressure is maintained in the source reservoir (occasionally a chamber), thereby providing the potential for a large eruption, through graben subsidence. The graben subsidence itself is regarded as primarily of tectonic origin.

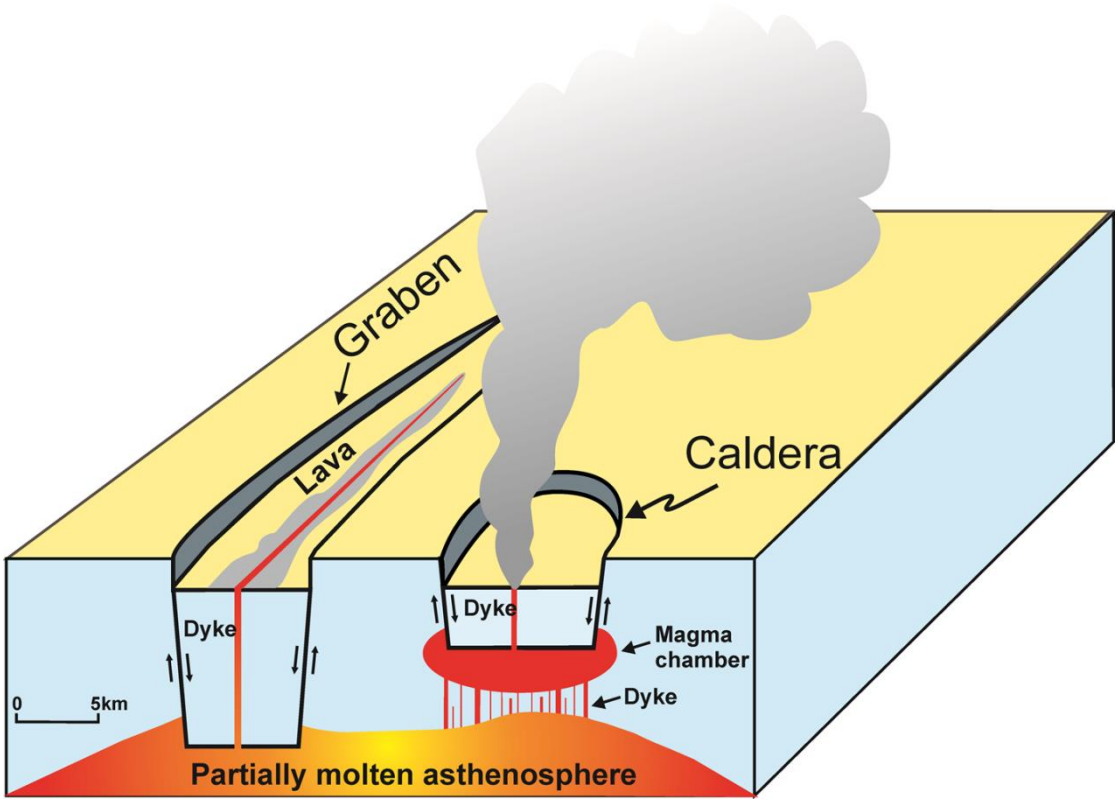

Fig. 18. *In the present models, large volcanic eruptions are generally related to graben subsidence (primarily effusive eruptions) and caldera subsidence (primarily explosive eruptions). Grabens and collapse calderas are mechanically analogous structures. Both relate to (primarily) dip-slip faults along which subsidence or vertical displacement of the crustal block in-between the faults occurs. Both result in temporary or permanent rapid reduction in the volume of the associated chamber/reservoir and may thus contribute to squeezing out a high proportion (sometimes all) of its magma during an eruption, thereby producing large eruptions.*

More specifically, in this paper I propose a new model for the generation of large to very large eruptions that is based on the principle of subsidence of a crustal block into the chamber/reservoir so as to maintain high excess pressure during the eruption. The model is basically the same for both explosive eruptions and effusive eruptions whereby the squeezing out of the magma is related to subsidence of a crustal block into the chamber/reservoir (Fig. 18). For explosive eruptions, the subsidence is normally related to the displacement of a caldera block, whereas for effusive eruptions the subsidence is normally related to the displacement of a graben block. The basic ideas, as to the similarity between the subsidence of collapse calderas and grabens, was presented earlier (Gudmundsson, 1999), but this is the first paper to explore the mechanical consequences of these similarities as a mechanism for generating large and very large explosive and effusive eruptions.

9.1 Explosive and effusive eruptions

While large explosive eruptions are normally associated with caldera collapses and large effusive eruptions with graben subsidences (Fig. 18), the opposite relation is also known. Thus, a caldera subsidence may give rise to a large effusive eruption, and a graben

subsidence can give rise to a large explosive eruption. For example, there is strong evidence from the Sierra Madre Occidental volcanic province that many ignimbrite (explosive) eruptions were related to graben subsidences. This province is located in Mexico, just south of its boundary with the United States, formed mostly 23-38 million years ago and has a cumulative ignimbrite volume of 580,000 km^3, making it the largest continuous ignimbrite province on Earth (Aguirre-Diaz et al., 2003, 2008). Also, rhyolite flows and acid tuffs were apparently erupted in connection with graben subsidence in Oregon (United States) about 15.4 million years ago (Cummings et al., 2000). Similarly, a major incremental subsidence is reported from the Snake River basins in Idaho (United States) during 12 major explosive rhyolitic eruptions (related to the Yellowstone hot spot) during the period from 11.3 to 8.1 Ma (Knott et al., 2016). In fact, the original volcanotectonic idea as to the formation of the Toba Caldera is that it forms the central, collapsed part of a very large dome-like structure. This structure, referred to as the Batak Tumor (van Bemmelen, 1939), is then supposed to be the result of magma accumulation beneath the large dome-like structure over a period of perhaps 1 Ma. In van Bemmelen's conceptual model, the resulting Toba Caldera has an inward-dipping (normal) ring-fault whereas others considered the caldera itself (partly at least) as a volcanotectonic graben (Chesner, 2012).

In case a crustal magma chamber is primarily basaltic, caldera collapse may result in a large basaltic effusive eruption. It should be noted, though, that none of the caldera collapses in basaltic edifices during the past hundred years or so has given rise to large basaltic eruptions. Thus, none of the four collapses in basaltic edifices, discussed above, namely Fernandina in 1968, Plosky Tolbachik in 1975-1976, Miyakejima in 2000, and Piton de la Fournaise in 2007 gave rise to large eruptions. For large effusive eruptions, therefore, graben subsidences are probably more common associated mechanical process than caldera collapse, even though both processes may, in principle, generate such eruptions.

9.2 Driving shear stress for fault slip

One result mentioned here, and discussed in detail earlier (Gudmundsson, 2014), is that the elastic strain energy released in the largest eruptions is of the same order of a magnitude as in the largest earthquakes recorded so far. This may be an indication of certain limits as to the strain-energy storage capacity of the Earth's crust before failure or, alternatively, the amount of strain energy that can be released from a crustal segment during a single event. Since the driving stresses (nominal stress drops) of earthquakes are very similar to the excess pressures of magma chambers before rupture and eruption, these similarities seem logical, although never demonstrated before. More specifically, the excess pressure at chamber rupture and the driving shear stress of an earthquake should, theoretically, differ by a factor of about 2. This is a consequence of the Modified Griffith Criterion for fault slip, namely (e.g., Gudmundsson, 2011):

$$\tau_d = 2T_0 + \mu_f \sigma_n \tag{35}$$

Here τ_d is the driving shear stress for the fault slip (roughly equal to the nominal stress drop associated with an earthquake), T_0 is the in-situ tensile strength of the rock, μ_f is the

coefficient of internal friction, and σ_n is the normal stress on the fault (or earthquake rupture) plane. Equation (35) is commonly used when describing the conditions for fault slip in laboratory experiments on small specimens; it applies in the absence of fluids, that is, to dry conditions. All tectonically active crustal segments, however, contain fluids (e.g., groundwater or geothermal water), and it is widely thought that there are no major earthquakes without high fluid pressures in the associated fault zone. In particular, volcanoes with highly porous rocks are commonly the sites of geothermal and groundwater fields. Furthermore, many ring-faults are injected by ring-dykes formed under high magmatic (fluid) overpressure (Figs. 10 and 12). Denote the total fluid pressure in the fault zone at the site of the potential rupture plane by p_t. Then Eq. (35) becomes:

$$\tau_d = 2T_0 + \mu_f (\sigma_n - p_t) \tag{36}$$

Except for very deep earthquakes, the driving shear stress τ_d in Eq. (36) is normally in the range of 1-10 MPa, and most commonly around 2-6 MPa (Kanamori and Anderson, 1975; Kanamori, 1977). This suggests that during most earthquakes, including those associated with slip on ring-faults, the term $\mu_f (\sigma_n - p_t)$ is close to or actually zero (and possibly negative, particularly during ring-dyke propagation, Fig. 12). Because μ_f is always positive, this implies that the term $(\sigma_n - p_t)$ is zero, so that the fluid pressure is equal to the normal stress σ_n on the rupture or fault plane (cf. Gudmundsson, 2011). It follows that for an earthquake rupture the driving shear stress is commonly equal to twice the in-situ tensile strength, or $2T_0$, whereas for the rupture of a magma chamber and dyke injection the excess pressure is equal to T_0 (Eq. 16). Since the in-situ tensile strength of crustal rocks is most commonly a few mega-pascals, as indicated above, the excess pressure in the magma chamber and the driving shear stress are likely to be mostly in the range of about 2-6 MPa, as is, indeed, observed.

9.3 Comparison with the underpressure model of collapse calderas

It is important to recognise that in the model presented here, for both calderas and grabens (Fig. 18), the subsidence is not the consequence of the eruption but rather the provider of the energy that squeezes out the magma and thus largely drives the eruption. This follows from the following observations:

- There is no known natural (spontaneous) mechanism whereby magma or other fluids flow from lower potential energy to higher potential energy. Thus, for example, there is no known way to generate large absolute ‘underpressure’ (pressure less than lithostatic) in a large part of a totally fluid magma chamber. Because in order to do so the magma would have to flow from a chamber at a lower total pressure into the host rock at a higher total pressure (Gudmundsson, 2008).
- Similarly, there is no known way to generate a geologically large empty cavity at the depth of many kilometres in the crust—say half an empty magma chamber—into which a collapse caldera (or possibly a graben) could collapse or subside. As indicated above, the in-situ shear strength of rocks is generally similar to the nominal stress drop or driving shear stress in earthquakes, the highest values being about 30 MPa (Scholz, 1990) and the most common values, except for very deep earthquakes,

1-10 MPa (Kanamori and Anderson, 1975; Kanamori, 1977). As indicated below, large stress differences (shear stresses) cannot normally be maintained at the margin of a totally fluid magma chamber (Gudmundsson, 2011).

- At a contact with a fluid magma chamber, where the minimum principal stress σ_3 is either zero or slightly negative (and thus negligible in comparison with the maximum principal compressive stress, σ_1) the shear stress is roughly half the maximum principal stress σ_1 (e.g., Gudmundsson, 2011). Already at 2 km depth the shear stress at the contact with the magma chamber would thus be around 25 MPa (assuming a crustal density of 2500 kg m^{-3}), and would increase by some 13-15 MPa for each kilometre by which the depth to the roof of the shallow magma-chamber increases (Fig. 3). There is thus no way that an empty cavity on the size of a magma-chamber (dimensions reaching kilometres) could exist at such a depth; long before a large empty cavity could form, the rock would fail in shear or, for downward bending of the roof, in tension.
- Models based on forced underpressure to generate collapse calderas estimate underpressures (negative excess pressures) as high as 205 MPa for the Katmai 1912 collapse, 312 MPa for the Pinatubo 1991 collapse, and 290 MPa for the 1968 Fernandina collapse (Stix and Kobayashi, 2008). The in-situ (field) shear strength of rocks is roughly double their tensile strength (Eq. 36). Numerous in-situ tensile strength measurements indicate a general range of 0.5 to 6 MPa; the highest in-situ value ever measured is 9 MPa (Gudmundsson, 2011). The in-situ shear strength is thus expected to be generally in the range of 1-12 MPa, which is very similar to the driving shear stress or nominal stress drop in earthquakes. As indicated above, the latter is normally in the range of 1-10 MPa (Kanamori and Anderson, 1975; Kanamori, 1977). Models that invoke underpressure of the order of tens or hundreds of mega-pascals to explain collapse calderas are thus assuming in-situ shear strengths of the rocks hosting the magma chambers that are 1-2 orders of magnitude larger than measured.
- The underpressure model certainly gives rise to shear-stress concentration, but the location of the maximum shear stress is not suitable for typical ring-fault formation. For underpressure the maximum shear stress at the surface, both for a spherical (circular) magma chamber as well as for a sill-like (oblate ellipsoidal) magma chamber, is above the centre of the chamber – not above its margins (Gudmundsson, 2007, 2008). Underpressure is probably a common mechanism for shallow pit craters, but, as indicated above, hardly for collapse calderas extending as crustal blocks to depths of many kilometres.

Thus, in contrast to the underpressure model, in the present model on subsidence-driven large eruptions it is the subsidence of the caldera or the graben block that maintains the excess pressure in the chamber/reservoir and thereby allows much larger proportion of the magma to flow out of the chamber/reservoir before the feeder-dyke closes at its bottom than is possible in ‘ordinary’ eruptions (Fig. 18). For the caldera/graben subsidence to take place, the most favourable mechanical condition (not needed for outward-dipping ring-faults, Fig. 12) is extension across the potential or existing boundary fault of the caldera/graben. For

calderas, the energy source of the extension is commonly slight doming of the chamber as a result of magma accumulation in a large reservoir at the bottom of the hosting volcanic field or volcanic system (Fig. 14; Gudmundsson, 1998, 1999). Such a doming is common prior to ring-fault displacement – as was, for example, demonstrated through geodetic measurements prior to the 2014 displacement on the Bardarbunga Caldera in Iceland (Browning and Gudmundsson, 2015a). Similar 'doming' or inflation, related to a rather deep-seated reservoir (7-8 km below the summit of the volcano), was detected for several months prior to the Piton de la Fournaise collapse in 2007 – although in that case, deflation had set in again just before the collapse itself (Michon et al., 2011; Fontaine et al., 2014). For a graben, the energy source is normally associated with the driving forces of the divergent plate movements (Fig. 16). Other energy sources for grabens include pull-apart movements (along strike-slip faults, including transform faults), plate bending at subduction zones, gravity gliding (e.g., above mantle plumes), and volcano spreading.

9.4 Sizes of fault displacements

The fault displacements must normally be large (at least many hundreds of meters) for the caldera ring-faults to have a chance of triggering large explosive eruptions. Grabens are commonly with much larger areas than calderas, so that the displacement needed to trigger a similar-volume eruption as from a caldera is proportionally smaller (Fig. 18). As indicated above, displacements of tens of metres in reasonably large grabens may trigger eruptions with volumes of tens of cubic kilometres. However, for eruptions of the order of hundreds of cubic kilometres, not to speak of thousands of kilometres, very large grabens and displacements of the order of hundreds of metres or more are needed.

Large displacements during eruptions on the caldera ring-faults are well documented and commonly reach hundreds of meters and, occasionally, more than a kilometre. No really large caldera eruptions have been documented by modern instruments, but it is not difficult for large calderas to reach displacements of a kilometre or more in large eruptions. One reason why large slips are easy on caldera faults is that they are commonly close to vertical (Fig. 5). A second reason is that they are commonly occupied by magma during the slip, that is, the forming ring-dyke (Fig. 12). The friction along the ring-fault is then minimal, and very large slips are easy.

To generate tens or hundreds of metres of vertical slip on the normal boundary faults of grabens is primarily a question of the size of the fault. Because the fault is through-going and extends from one free surface (Earth's surface) to another one (the magma reservoir, in case the top region below the graben is assumed fluid), we use mode III model (Figs. 15 and 18; cf. Gudmundsson, 2011). Then the length or strike-dimension is the controlling dimension. For reasonable values of static Young's modulus, Poisson's ratio, and stress drop (driving shear stress), a 50 km long fault could slip by as much as 30 m in a single event. Some large flood basalts took 5-15 years to form (e.g. Self et al., 1997), in which case many slips on the graben faults would be possible. For grabens that are 100-150 km long the displacement in a single slip could reach 60-90 m. This is similar to the estimated maximum slip on the 2011 Tohoku (Japan) earthquake (Ito et al., 2011). Any pressure change in the associated magma reservoir would tend to concentrate stresses at the boundary faults (Fig. 15), particularly if, as is common, they have compliant cores and inner damage zones whose mechanical properties

are widely different from those of the host rocks (Gudmundsson, 2011). Under such conditions, the faults act as soft elastic inclusions.

No really large and well-monitored flood-basalt eruptions have occurred in historical time. Among the largest ones are the 934 Eldgja and the 1783 Laki eruptions in Iceland (Fig. 7). It is not known for either if there were graben subsidences prior to or during the early stages of these eruptions, partly because such grabens would have been largely or entirely buried by the subsequent lava flows. Laki has a small graben in its central part, but only about 300 m wide and with vertical displacements of several metres. It is too small to have had a significant effect on excess pressure in a deep-seated reservoir. Eldgja has a much larger graben. It is as wide as 600 m, about 150 m deep, and its central part (the one usually referred to as Eldgja) is about 8.5 km long. However, Eldgja itself is only the middle one of a row of offset graben segments, extending for about 40 km. Eldgja is a mixture of a graben and explosive craters, and its formation is not entirely clear. Nevertheless, much of it has a clear graben structure, perhaps with a total subsidence volume of 1-2 km^3. There are several other grabens in the areas of Eldgja and Laki that could have contributed to the excess pressures in the reservoirs, thereby generating comparatively large eruptive volumes.

It is remarkable that there are no lava shields in the East Volcanic Zone of Iceland (Fig. 7). By contrast, the largest fissure-generated Holocene lava flows have come from that zone. We have already discussed the comparatively large lava flows of Laki and Eldgja, both of which are historical (which in Iceland means younger than 1100 years). The largest Holocene lava flow in Iceland, however, is the Thjorsarhraun lava flow (Fig. 7; cf. Hjartarson, 1988) which issued from a fissure in the northern part of the East Volcanic Zone at around 8600 B.P. This site coincides with the largest graben in the East Volcanic Zone, namely the Heljargja Graben (Fig. 7). Strictly, Heljargja itself is primarily the graben that is located in Pleistocene rocks, mainly hyaloclastites, but it has been reactivated in Holocene lava flows, of different ages. The entire graben system, partly dissecting Pleistocene rocks and partly Holocene lava flows, is about 60 km long and as wide as 10 km. In places the subsidence is as great as 100 m (A.T. Gudmundsson, 2001). A graben system with an area of, say, 500 km^2, with fault slip of 50 m would generate a subsidence volume of 25 km^3. This is the same as the estimated volume of the Thorsarhraun lava, 25 km^3 (Hjartarson, 1988). There is of course not a one-to-one correspondence between the graben subsidence and the associated volume of the erupted lava. The reservoir is partially molten, and part of the melt may flow away from the feeder-dyke rather than towards it. Also, elastic and brittle deformation mechanisms imply that part of the subsidence volume is taken up in ways different from that of the reservoir volume decrease. Nevertheless, the fact that the largest Holocene lava flow in Iceland originated close to one of the largest graben systems in the volcanic zones of Iceland may indicate a connection along the lines discussed here.

10.Conclusions

The main results of this work may be summarised as follows:

- Common or ‘ordinary’ explosive and effusive eruptions are very small in comparison with the largest ones. Here eruptive volumes (V_{er}) of 0.1 km^3 or less are regarded as small, those in the range of 0.1-10 km^3 are regarded as moderate, and those larger

than 10 km^3 as large, with the largest ones reaching 10^3 km^3. Magma chambers are regarded as shallow if their roofs are at depths of 5 km or less. Magma sources for volcanoes located at greater depths are referred to as magma reservoirs. These are commonly much larger than, and supply magma to (feed), the shallow chambers.

- Typical orders of magnitudes of eruptive volumes in single eruptions are from 0.01 km^3 to 1 km^3, that is, small to moderate. Eruptions of these volumes can normally be explained in terms of poroelasticity, a theory widely used in hydrogeology, reservoir engineering, soil mechanics, and related fields.
- For a totally molten crustal magma chamber, the typical ratio between eruptive mafic materials and the volume of the chamber is $V_{er} \approx 7\times10^{-4}V_t$. In extreme cases when the magma chamber is composed entirely of gas-rich acid magma this ratio may be as large as $V_{er} \approx 4\times10^{-2}V_t$. However, both ratios assume a totally molten magma chamber, whereas many and presumably most chambers are partially molten, implying that the ratios are normally lower. Crustal magma chambers supplying magma to polygenetic volcanoes are generally thought to have volumes between 5 and 500 km^3, and commonly larger than 20 km^3 (chambers at fast-spreading ocean ridges may be smaller, however). For the largest chamber, of 500 km^3, the typical ratio for a totally molten mafic chamber would yield an eruptive volume of 0.35 km^3. To reach an eruptive volume of 1 km^3 would require a totally molten chamber of more than 1400 km^3.
- For large eruptions, of the order of 10^1 or more, a different mechanism is normally needed. The mechanism proposed and discussed here is chamber/reservoir volume reduction or shrinkage during the eruption through caldera/graben subsidence. The basic idea is that volcanotectonic stresses generate a ring-fault/graben boundary faults. When large slips occur on these faults during an eruption, the subsiding crustal block reduces the volume of the underlying chamber/reservoir, thereby maintaining the excess pressure in the chamber for a much longer time than is possible in the ordinary poroelastic mechanism. As a consequence a much higher proportion of the magma in the chamber/reservoir is driven or squeezed out during an eruption associated with caldera or graben subsidence than is normally possible. It follows that the volume of eruptive materials, $V_{er,}$ may approach the total volume of the chamber/reservoir, V_t that is, $V_{er} \rightarrow (0.1-1)V_t$, resulting in a large to very large eruption.
- This new mechanism for large eruptions implies that the basic physics of caldera subsidence and volcanotectonic graben subsidence is the same. The geometric difference in the surface expression of these structures is primarily related to cross-sectional shape of the underlying magma body. In the case of a collapse caldera, the underlying body—usually a shallow magma chamber—has a cross section that is either close to circular or somewhat elliptical in plan view. In the case of a graben, the underlying magma body—usually a deep-seated magma reservoir—is normally highly elongated along the axis of the associated rift zone.

- In this new mechanism, the large eruption is the consequence—not the cause—of the subsidence of the caldera/graben block. Thus, once the conditions for large-scale subsidence of a caldera/graben block are established during a particular unrest/rifting episode, primarily using geodetic and seismic data, then the likelihood of a large to very large eruptions can be assessed and used for reliable forecasting.

Acknowledgements

I thank Shigekazu Kusumoto, two anonymous reviewers, and Editor Arturo Gomez-Tuena for very helpful comments on an earlier version of this paper. I also thank Tim Horscroft, Review Papers Coordinator, for the original invitation to write a paper on this topic.

References

Acocella, V., 2007. Understanding caldera structure and development: and overview of analogue models compared to natural calderas. Earth-Science Reviews, 85, 125-160.

Aguirre-Diaz, G.J., Labarthe-Hernandez, G., 2003. Fissure ignimbrites: fissure-source origin for voluminous ignimbrites of the Sierra Madre Occidental and its relationship with Basin and Range faulting. Geology, 31, 773-776.

Aguirre-Diaz, G.J., Labarthe-Hernandez, G., Tristan-Gonzalez, M., Nieto-Obregon, J., 2008. Graben-calderas of the Sierra Madre Occidental, Mexico. In: J. Marti and J. Gottsmann (eds.), Caldera Volcanism: Analysis, Modelling and Response. Workshop, Tenerife, Spain, p. 6.

Almond, D.C. 1977. The Sabaloka igneous complex, Sudan. Phil. Trans. Roy. Soc. Lond., A287, 595-633.

Amelung, F., Jonsson, S., Zebker, H., Segall, P., 2000. Widespread uplift and `trapdoor' faulting on Galapagos volcanoes observed with radar interferometry. Nature, 407, 993-996.

Anderson, E. M., 1936. The dynamics of formation of cone sheets, ring dykes and cauldron subsidences. Proceedings of the Royal Society of Edinburgh, 56, 128-163.

Andrew, R.E.B., Gudmundsson, A., 2007. Distribution, structure, and formation of Holocene lava shields in Iceland. Journal of Volcanology and Geothermal Research, 168, 137-154.

Annen, C. 2011. Implications of incremental emplacement of magma bodies for magma differentiation, thermal aureole dimensions and plutonism-volcanism relationships. Tectonophysics, 500, 3-10.

Arnadottir, T., Geirsson, H., Jiang, W., 2008. Crustal deformation in Iceland: plate spreading and earthquake deformation. Jokull, 58, 59-74.

Aramaki, S. 1984. Formation of the Aira caldera, southern Kyushu, ~ 22,000 years ago. Journal of Geophysical Research, 89, 8484-8501.

Bear, J., 1972. Dynamics of Fluids in Porous Media. Elsevier, Amsterdam.

Becerril, L., Galindo, I., Gudmundsson, A., Morales, J.M., 2013. Depth of origin of magma in eruptions. Scientific Reports 3, 2762. doi: 10.1038/srep02762

Blake, S., 1981. Volcanism and the dynamics of open magma chambers. Nature, 289, 783-785.

Blake, S., 1984 Volatile oversaturation during the evolution of silicic magma chambers as an eruption trigger. Journal of Geophysical Research, 89, 8237– 8244.

Brandsdottir, B., Menge, W.H., 2008. The seismic structure of Iceland. Jokull, 58, 17-34.

Branney, M.J. 1995. Downsag and extension at calderas: new perspectives on collapse geometries from ice-melt, mining, and volcanic subsidence. Bulletin of Volcanology, 57, 303-318.

Browning, J., Gudmundsson, A., 2015a. Surface displacements resulting from magma-chamber roof subsidence, with application to the 2014–2015 Bardarbunga–Holuhraun volcanotectonic episode in Iceland. Journal of Volcanology and Geothermal Research, 308, 82–98.

Browning, J., Gudmundsson, A., 2015b. Caldera faults capture and deflect inclined sheets: An alternative mechanism of ring-dike formation. Bulletin of Volcanology, 77, 889, doi: 10.1007/s00445-014-0889-4.

Bull, J.M., Minshull, T.A., Mitchell, N.C., Thors, K., Dix, J.K., Best, A.I., 2003. Fault and magmatic interaction within Iceland's western rift over the last 9 kyr. Geophysical Journal International, 154, F1-F8.

Burov, E.B., Guillou-Frottier, L., 1999. Thermomechanical behavior of large ash flow calderas. Journal of Geophysical Research, 104, 23,081-23,109.

Burov, E., Jaupart, C., Guillou-Frottier, L., 2003. Ascent and emplacement of buoyant magma bodies in brittle-ductile upper crust. Journal of Geophysical Research, 108, 2177, doi:10.1029/2002JB001904.

Carey, S.N., Sigurdsson, H. ,1989. The intensity of plinian eruptions. Bulletin of Volcanology, 51, 28-40.

Caricchi, L., Annen, C., Blundy, J., Simpson, G., Pinel, V., 2014. Frequency and magnitude of volcanic eruptions controlled by magma injection and buoyancy. Nature Geoscience, 7, 126-130, doi:10.1038/ngeo2041.

Chaussard, E., Amelung, F., 2014. Regional controls on magma ascent and storage in volcanic arcs. Geochemistry, Geophysics, Geosystems, 15, doi:10.1002/2013GC005216.

Chesner, C.A., Rose, W.I., Deino, A., Drake, R., Westgate, J.A., 1991. Eruptive history of Earth's largest Quaternary caldera (Tobe, Indonesia) clarified. Geology, 19, 200-203.

Chesner, C.A., 2012. The Toba Caldera Complex. Quaternary International, 258, 5-18.

Clauset, A., Chalizi, R.C., Newman, M.E.J., 2009. Power-law distributions in empirical data. Society for Industrial and Applied Mathematics, 51, 661–703.

Cole, J.W., Milner, D.M., Spinks, K.D. 2005. Calderas and caldera structures: a review. Earth Science Review, 69, 1-26.

Costa, A., Gottsmann, J., Melnik, O., Sparks, R.S.J., 2011. A stress-controlled mechanism for the intensity of very large magnitude explosive eruptions. Earth and Planetary Science Letters, 310, 161-166, doi:10.1016/j.epsl.2011.07.024.

Crosweller, H.S., Arora, B., Brown, S.K, Cottrell, E., Deligne, N.I., Guerrero, N.O., Hobbs, L., Kiyosugi, K., Loughlin, S.C., Lowndes, J., Nayembil, Siebert, L., Sparks, R.S.J., Takarada, S., and Venzke, E., 2012. Global database on large magnitude explosive volcanic eruptions (LaMEVE). Journal of Applied Volcanology, 1:4, doi; 10.1186/2191-5040-1-4.

Cummings, M.L., Evans, J.G., Ferns, M.L., Lees, K.R., 2000. Stratigraphic and structural evolution of the middle Miocene synvolcanic Oregon-Idaho graben. Geological Society of America Bulletin, 112, 668-682.

de Silva, S. L., Gosnold, W.D., 2007. Episodic construction of batholiths: Insights from the spatiotemporal development of an ignimbrite flare-up. Journal of Volcanology and Geothermal Research, 167, 320-335, doi:10.1016/j.jvolgeores.2007.07.015.

de Silva, S. L., Gregg, P.M.., 2014. Thermomechanical feedbacks in magmatic systems: Implications for growth, longevity, and evolution of large caldera-forming magma reservoirs and their supereruptions, Journal of Volcanology and Geothermal Research, 282, 77-91, doi:10.1016/j.jvolgeores.2014.06.001.

Dobran, F., 2001. Volcanic Processes: Mechanisms in Material Transport. Springer Verlag, Berlin.

Elder, J.W., 1976. The Bowels of the Earth. Oxford University Press, Oxford.

Fedotov, S.A., 1985. Estimates of heat and pyroclast discharge by volcanic eruptions based upon the eruption cloud and steady plume observations. Journal of Geodynamics, 3, 275-302.

Fedotov, S.A., Chirkov, A.M., Gusev, N.A., Kovalev, G.N., Slezin, Yu.B., 1980. The large fissure eruption in the region of Plosky Tolbachik Volcano in Kamchatka, 1975-1976. Bulletin of Volcanology, 43, 47-60.

Fialko, Y. A., Rubin, A.M., 1998. Thermodynamics of lateral dike propagation: Implications for crustal accretion at slow spreading mid-ocean ridges, Journal of Geophysical Research, 103, 2501-2514.

Filson, J., Simkin, T., Leu, L. 1973. Seismicity of a caldera collapse: Galapagos Islands 1968. Journal of Geophysical Research, 78, 8591-8622.

Folch, A., Marti, J., 1998. The generation of overpressure in felsic magma chambers by replenishment, Earth and Planetary Science Letters, 163, 301-314, doi:10.1016/s0012-821x(98)00196-4.

Folch, A., Marti, J., 2004. Geometrical and mechanical constraints on the formation of ring-fault calderas, Earth and Planetary Science Letters, 221, 215-255.

Fontaine, F.R., Roult, G., Michon, L., Barruo, G., Di Muro, A., 2014. The 2007 eruptions and caldera collapse of the Piton de la Fournaise volcano (La Reunion Island) from tilt analysis at a single very broadband seismic station. Geophysical Research Letters, 41, 2803-2811, doi:10.1002.grl.v.41.8.

Galindo, I., Gudmundsson, A., 2012 Basaltic feeder-dykes in rift zones: geometry, emplacement, and effusion rates. Natural Hazards and Earth System Sciences, 12, 3683–3700.

Gautneb, H., Gudmundsson, A., Oskarsson, N., 1989. Structure, petrochemistry, and evolution of a sheet swarm in an Icelandic central volcano. Geol. Mag., 126, 659-673.

Gelman, S. E., Gutierrez, F.J., Bachmann, O., 2013. On the longevity of large upper crustal silicic magma reservoirs, Geology, 41, 759-762, doi:10.1130/g34241.1.

Gerbault, M., Cappa, F., Hassani, R., 2012. Elasto-plastic and hydromechanical models of failure around an infinitely long magma chamber. Geochemistry Geophysics Geosystems, 13, doi:10.1029/2011gc003917.

Geshi, N., Shimano, T., Chiba, T., Nakada, S. 2002. Caldera collapse during the 2000 eruption of Miyakejima Volcano, Japan. Bulletin of Volcanology, 64, 55-58.

Geyer, A., Marti, J., 2008. The new worldwide collapse caldera database (CCDB): A tool for studying and understanding caldera processes. Journal of Volcanology and Geothermal Research, 175, 334-354

Geyer, A., Marti, J., 2014. A short review of our current understanding of the development of ring faults during collapse caldera formation. Frontiers in Earth Science, 2: 22. doi:10.3389/feart.2014.00022.

Gonnermann, H.M., Manga, M., 2013. Dynamics of magma ascent in the volcanic conduit. In: Fagents, S.A., Gregg, T.K.P., Lopes, R.M.C. (eds), Modeling Volcanic Processes. Cambridge University Press, Cambridge, pp. 55-84.

Greenland, L.P., Rose, W.I., Stokes, J.B., 1985. An estimate of gas emissions and magmatic gas content from Kilauea volcano. Geochimica et Cosmochimica Acta, 49, 125-129.

Greenland, L. P., Okamura, A. T., Stokes, J. B., 1988. Constraints on the mechanics of the eruption. In: Wolfe, E. W (ed), The Puu Oo Eurption of Kilauea Volcano, Hawaii: Episodes Through 20, January 3, 1983 Through June 8, 1984, US Geol. Survey Professional Paper, 1463, 155–164.

Gregg, P.M., de Silva, S.L., Grosfils, E.B., Parmigiani, J.P., 2012. Catastrophic caldera-forming eruptions: Thermomechanics and implications for eruption triggering and maximum caldera dimensions on Earth. Journal of Volcanology and Geothermal Research 241-242, 1-12.

Gregg, P.M., de Silva, S.L., Grosfils, E.B., 2015. Catastrophic caldera-forming eruptions II: The subordinate role of magma buoyancy as an eruption trigger. Journal of Volcanology and Geothermal Research, 305, 100-113.

Grosfils, E. B., 2007. Magma reservoir failure on the terrestrial planets: Assessing the importance of gravitational loading in simple elastic models. Journal of Volcanology and Geothermal Research, 166, 47-75, doi:10.1016/j.jvolgeores.2007.06.007.

Gudmundsson, A., 1986. Mechanical aspects of postglacial volcanism and tectonics of the Reykjanes Peninsula, southwest Iceland. Journal of Geophysical Research, 91, 12,711-12,721.

Gudmundsson, A., 1987a. Formation and mechanics of magma reservoirs in Iceland. Geophysical Journal of the Royal Astronomical Society, 91, 27-41.

Gudmundsson, A., 1987b. Tectonics of the Thingvellir fissure swarm, SW Iceland. Journal of Structural Geology, 9, 61-69.

Gudmundsson, A., 1990. Emplacement of dikes, sills and crustal magma chambers at divergent plate boundaries. Tectonophysics, 176, 257-275.

Gudmundsson, A. 1998. Formation and development of normal-fault calderas and the initiation of large explosive eruptions. Bulletin of Volcanology, 60, 160-170.

Gudmundsson, A., 1999. Explosive eruptions triggered by dip slip on caldera faults. Volcanology and Seismology 20, 239-254.

Gudmundsson, A., 2006. How local stresses control magma-chamber ruptures, dyke injections, and eruptions in composite volcanoes. Earth-Science Reviews, 79, 1-31.

Gudmundsson, A., 2007. Conceptual and numerical models of ring-fault formation. Journal of Volcanology and Geothermal Research, 164, 142-160.

Gudmundsson, A., 2008. Magma-chamber geometry, fluid transport, local stresses, and rock behaviour during collapse-caldera formation. In: Gottsmann, J., Marti, J. (eds.), Caldera Volcanism: Analysis, Modelling and Response. Developments in Volcanology 10. Elsevier, Amsterdam, pp. 313-349.

Gudmundsson, A., 2011. Rock Fractures in Geological Processes. Cambridge, Cambridge University Press.

Gudmundsson, A., 2012. Magma chambers: formation, local stresses, excess pressures, and compartments. Journal of Volcanology and Geothermal Research, 237-238, 19–41.

Gudmundsson, A., 2014. Energy release in great earthquakes and eruptions. Frontiers in Earth Science 2:10. doi: 10.3389/feart.2014.00010.

Gudmundsson, A., 2015. Collapse-driven large eruptions. Journal of Volcanology and Geothermal Research, 304, 1-10.

Gudmundsson, A., Mohajeri, N., 2013. Entropy and order in urban street networks. Scientific Reports 3:3324. doi:10.1038/srep03324.

Gudmundsson, A.T., 2001. Icelandic Volcanoes. Reykjavik, Vaka-Helgafell (in Icelandic).

Guo, X., 2013. Density and Compressibility of FeO-bearing Silicate Melt: Relevance to Magma Behavior in the Earth. PhD Thesis, University of Michigan, Ann Arbor, Michigan.

Haimson, B.C., Rummel, F., 1982. Hydrofracturing stress measurements in the Iceland research drilling project drill hole at Reydarfjordur, Iceland. Journal of Geophysical Research, 87, 6631-6649.

Hedervari, P., 1963. On the energy and magnitude of volcanic eruptions. Bulletin of Volcanology, 25, 374-385.

Hildreth, W., Fierstein, J., 2012. The Novarupta-Katmai eruption of 1912—largest eruption of the twentieth century; centennial perspectives: U.S. Geological Survey Professional Paper 1791, 259 pp.

Hjartarson, A., 1988. The great Thjorsa lava – the largest Holocene lava flow. Natturufraedingurinn, 58, 1-16 (in Icelandic).

Holohan, E. P., de Vries, B.C., Troll, V.R., 2008. Analogue models of caldera collapse in strike-slip tectonic regimes, Bulletin of Volcanology, 70, 773-796, doi:10.1007/s00445-007-0166-x.

Holohan, E. P., Troll, V.R., Walter, T.R., Munn, S., McDonnell, S., Shipton, Z.K., 2005. Elliptical calderas in active tectonic settings: an experimental approach, Journal of Volcanology and Geothermal Research, 144, 119-136, doi:10.1016/j.jvolgeores.2004.11.020.

Hooper, R.R., Camp, V.E., Reidel, S.P., Ross, M.E., 2007. The origin of the Columbia River flood basalt province: plumes versus nonplumes models. In: Foulger, G.R., Jurdy, D.M., eds, Plates, Plumes, and Planetary Processes. Geological Society of American Special Paper 430, pp. 635-668, doi: 10.1130/2007.2430(30)

Hughes, G. R., Mahood, G.A., 2011. Silicic calderas in arc settings: Characteristics, distribution, and tectonic controls, Geol. Soc. Am. Bull., 123, 1577-1595, doi:10.1130/b30232.1.

Ito, T., Ozawa, K., Watnabe, T., Sagiya, T., 2011. Slip distributionof the 2011 off the Pacific coast of Tohoku Earthquake inferred from geodetic data. Earth Planets Space, 63, 627-630.

Jaxybulatov, K., Shapiro, N.M., Koulakov, I., Mordret, A., Landes, M., Sens-Schonfelder, C., 2014. A large magmatic sill complex beneath the Toba caldera. Science, 346, 617-619, doi: 10.1126/science.1258582.

Kanamori, H., 1977. The energy release in great earthquakes. Journal of Geophysical Research, 82, 2981-2987.

Kanamori, H., Anderson, D.L., 1975. Theoretical basis of some empirical relations in seismology. Bulletin of the Seismological Society of America, 65, 1074-1095.

Karlstrom, L., Dufek, J., Manga, M., 2010. Magma chamber stability in arc and continental crust. Journal of Volcanology and Geothermal Research, 190, 249-270, doi:10.1016/j.jvolgeores.2009.10.003.

Karlstrom, L., Rudolph, M.L., Manga, M., 2012. Caldera size modulated by the yield stress within a crystal-rich magma reservoir, Nature Geoscience, DOI: 10.1038/NGEO1453.

Knott, T.T., Brenney, M.J., Reichow, M.K., Finn, D.R., Coe, R.S., Storey, M., Barfod, D., McCurry, M., 2016. Mid-Miocene record of large-scale Snake-River-type explosive volcanism and associated subsidence on the Yellowstone hotspot track: the Cassia Formation of Idaho, USA. Geological Society of America Bulletin, doi: 10.1130/B31324.1.

Kress, V.C., Carmichael, I.S.E., 1991. The compressibility of silicate liquids containing Fe2O3 and the effect of composition, temperature, oxygen fugacity and pressure on their redox states. Contributions to Mineralogy and Petrology, 108, 82–92.

Kumagai, H., Ohminato, T., Nakano, M., Ooi, M., Kubo, A., Oikawa, J., 2001. Very-long-period seismic signals and caldera formation at Miyake Island, Japan. Science, 293, 687-690.

Kusumoto, S., Takemura, K., 2005. Caldera geometry determined by the depth of the magma chamber. Earth Planets Space, 57, e17-e20.

Kusumoto, S., Gudmundsson, A., 2009. Magma-chamber volume changes associated with ring-fault initiation using a finite-sphere model: Application to the Aira caldera, Japan. Tectonophysics, 471, 58-66.

Lamb, H., 1932. Hydrodynamics, 6th ed. Cambridge University Press, Cambridge.

Lavallee, Y., de Silva, S.L., Salas, G., Byrnes, J.M., 2006). Explosive volcanism (VEI 6) without caldera formation: insight from Huaynaputina volcano, southern Peru, Bulletin of Volcanology, 68, 333-348, doi:10.1007/s00445-005-0010-0

Lipman, P.W. 1984. The roots of ash flow calderas in western North America: windows into the tops of granitic batholiths. Journal of Geophysical Research, 89, 8801-8841.

Lipman, P.W. 1997. Subsidence of ash-flow calderas: relation to caldera size and magma chamber geometry. Bulletin of Volcanology, 59, 198-218.

Macdonald, G.A. 1972.Volcanoes. Prentice-Hall, New Jersey.

Machado, F., 1974. The search for magmatic reservoirs. In: Civetta, L., Gasparini, P., Luongo, G., Rapolla, A. (eds.), Physical Volcanology, Elsevier, Amsterdam, pp. 255-273.

Malfait, W.J., Sanchez-Valle, C., Ardia,P., Médard, E., Lerch, P., 2011. Compositional dependent compressibility of dissolved water in silicate glasses.American Mineralogist, 96, 1402–1409.

Marti, J., Gudmundsson, A., 2000. The Las Canadas caldera (Tenerife, Canary Islands): Example of an overlapping collapse caldera generated by magma-chamber migration. Journal of Volcanology and Geothermal Research, 103, 161-173.

Marti, J., Ablay, G.J., Redshaw, L.T., Sparks, R.S.J., 1994. Experimental studies of collapse calderas. Journal Geological Society London, 151, 919-929.

Marti, J., Geyer, A., Folch, A., Gottsmann, J., 2008. A review on collapse caldera modelling. In: Gottsmann, J. and Marti, J. (eds), Caldera Volcanism: Analysis, Modelling and Response. Elsevier, Amsterdam, pp 233-283

Marti, J., Geyer, A., Folch, A., 2009. A genetic classification of collapse calderas based on field studies, and analogue and theoretical modelling. In: Thordarson, T., Self, S. (eds), Volcanology: the Legacy of GPL Walker. IAVCEI-Geological Society of London, London, pp. 249-266.

Mason, B.G., Pyle, D.M., Oppenheimer, C., 2004. The size and frequency of the largest explosive eruptions on Earth. Bulletin of Volcanology, 66, 735-748, doi: 10.1007/s00445-004-0355-9.

Michel, J., Baumgartner, L., Putlitz, B., Schaltegger, U., Ovtcharova, M., 2008. Incremental growth of the Patagonian Torres del Paine laccolith over 90 k.y. Geology, 36, 459-462, doi: 10.1130/G24546A.1.

Michon, L., Massin, F., Famin, V., Ferrazzini, V., Roult, G., 2011. Basaltic calderas: collapse dynamics, edifice deformation, and variations in magma withdrawal. Journal of Geophysical Research, 116, doi: 1029/2010JB007636.

Milne-Thompson, L.M., 1996. Theoretical Hydrodynamics, 5th ed. Dover, New York.

Mohajeri, N., Gudmundsson, A., 2014. The evolution and complexity of urban street networks. Geographical Analysis, 46, 345–367.

Murase, T., McBirney, A.R., 1973. Properties of some common igneous rocks and their melts at high temperatures. Geological Society of America Bulletin, 84, 3563-3592.

Neri, M., Acocella, V., Behncke, B., Giammanco, S., Mazzarini, F., Rust, D., 2011. Structural analysis of the eruptive fissures at Mount Etna (Italy). Annals of Geophysics, 54, 464-479, doi: 10.4401/ag-5332

Newhall, C.G., Dzurisin, D., 1988. Historical Unrest of Large Calderas of the World. U.S. Geological Survey Bulletin 1855, Reston, VA.

Newhall, C., Hendley II, J.W., Stauffer, P.H., 1997. The Cataclysmic 1991 Eruption of Mount Pinatubo, Philippines. U.S. Geological Survey Fact Sheet 113-97.

Newhall, C.G., Self, S., 1982. The volcanic explosivity index (VEI)—an estimate of explosive magnitude for historical volcanism. Journal of Geophysical Research, 87, 1231-1238.

Ochs, F.A., Lange, R.A., 1997. The partial molar volume, thermal expansivity, and compressibility of H2O in NaAlSi3O8 liquid: new measurements and an internally consistent model. Contributions to Mineralogy and Petrology, 129, 155-165.

Oftedahl, C. 1953. The igneous rock complex of the Oslo region: XIII. The cauldrons. Skrifter Det Norske Videnskaps-Akademi i Oslo, 3, 1-108.

Pisarenko, V., Rodkin, M., 2010. Heavy-Tailed Distributions in Disaster Analysis. Springer Verlag, Berlin.

Pyle, D.M., 1995. Mass and energy budgets of explosive volcanic eruptions. Geophysical Research Letters, 22, 563-566.

Pyle, D.M., 2000. Sizes of volcanic eruptions. In: Sigurdsson, H. et al. (eds.), Encyclopedia of Volcanoes. New York: Academic Press, pp. 263-269.

Reidel, S.P., Tolan, T.L., Hooper, P.R., Beeson, M.H., Fecht, K.R., Bentley, R.D. and Anderson, J.L., 1989. The Grande Ronde Basalt, Columbia River Basalt Group; stratigraphic descriptions and correlations in Washington, Oregon and Idaho. In: Reidel, S.P., and Hooper, P.R., eds., Volcanism and Tectonism in the Columbia River Flood-basalt province: Geological Society of America Special Paper 239, pp. 293-306.

Roche, O., Druitt, T.H., 2001. Onset of caldera collapse during ignimbrite eruptions, Earth and Planetary Science Letters, 191, 191-202.

Rosi, M., Papale, P., Lupi, L., and Stoppato, M., 2003. Volcanoes: Buffalo, Firefly Books.

Rossi, M.J., 1996. Morphology and mechanism of eruption of postglacial lava shields in Iceland. Bulletin of Volcanology 57, 530–540.

Saemundsson, K., 1992. Geology of the Thingvallavatn area. Oikos 64, 40–68.

Scholz, C.H., 1990. The Mechanics of Earthquakes and Faulting. Cambridge University Press, Cambridge.

Seifert, R., 2013 Compressibility of Volatile-bearing Magmatic Liquids. PhD Thesis, ETH, Zurich.

Self, S., Rampino, M.R., Newton, M.S., Wolff, J.A., 1984. Volcanological study of the great Tambora eruption of 1815. Geology, 12, 659-663.

Self, S., Thordarson, T., and Keszthelyi, L., 1997, Emplacement of continental flood basalt lava flows, in Mahoney, J.J., Coffin, M.F., eds., Large Igneous Provinces: Continental, Oceanic, and Planetary Flood Volcanism: American Geophysical Union Monograph 100, p. 381-410

Schultz, R.A., 1995. Limits on strength and deformation properties of jointed basaltic rock masses. Rock Mech. Rock Eng. 28, 1-15.

Simakin, A. G., Ghassemi, A., 2010. The role of magma chamber-fault interaction in caldera forming eruptions. Bulletin of Volcanology, 72, 85-101, doi:10.1007/s00445-009-0306-6.

Simkin, T., Howard, K.A. 1970. Caldera collapse in the Galapagos Islands, 1968. Science, 169, 429-437.

Simkin, T., Siebert, L., 2000. Earth's volcanoes and eruptions: an overview. In: Encyclopaedia of Volcanoes (ed. Sigurdsson, H.), p. 249-261, New York, Academic Press.

Sinton, J., Gronvold, K., Saemundsson, K., 2005. Postglacial eruptive history of thewestern Volcanic Zone, Iceland. Geochemistry Geophysics Geosystems 6, Q12009. doi:10.1029/2005GC001021.

Smil, V., 2008. Energy in Nature and Society: General Energetics of Complex Systems. MIT Press, London.

Sommerfeld, A., 1964. Thermodynamics and Statistical Mechanics. Academic Press, London.

Sonnette, L., Angelier, J., Villemin, T., Bergerat, F., 2010. Faulting and fissuring in active oceanic rift: Surface expression, distribution and tectonic–volcanic interaction in the Thingvellir Fissure Swarm, Iceland. Journal of Structural Geology, 32, 407–422, doi:10.1016/j.jsg.2010.01.003.

Sparks, R.S.J., Bursik, M.I., Carey, S.N., Gilbert, J.S., Glaze, L.S., Sigurdsson, H., Woods, A.W., 1997. Volcanic Plumes. Wiley, New York.

Stasiuk, M.V., Jaupart, C., Sparks, R.S.J., 1993. On the variation of flow rate in non-explosive lava eruptions. Earth and Planetary Science Letters, 114, 505-516.

Stix, J., Kobayashi, T., 2008. Magma dynamics and collapse mechanisms during four historic eruptions. Journal of Geophysical Research, 113, doi: 1029/2007JB005073.

Stothers, R.B., 1984, The great Tambora eruption in 1815 and its aftermath. Science, 224, 1191-1198.

Thordarson, T., Larsen, G., 2007. Volcanism in Iceland in historical time: volcano types, eruption styles and eruptive history. Journal of Geodynamics, 43, 118-152.

Thordarson, T., Hoskuldsson, A., 2008. Postglacial volcanism in Iceland. Jokull, 58, 197-228.

Thordarson, T., Self, S., 1993. The Laki (Skaftar Fires) and Grimsvotn eruptions in 1783-1785. Bulletin of Volcanology, 55, 233-263.

Tolan, T.L., Reidel, S.P., Beeson, M.H., Anderson, J.L., Fecht, K.R., and Swanson, D.A., 1989. Revisions to the estimates of the areal extent and volume of the Columbia River Basalt Group. In: Reidel, S.P., and Hooper, P.R., eds., Volcanism and Tectonism in the Columbia River Flood-basalt province. Geological Society of America Special Paper 239, pp. 1-20.

Tryggvason, E., 1982. Recent ground deformation in continental and oceanic rift zones. In: Palmason, G. (Ed.), Continental and Oceanic Rifts. Geodynamic Series, vol. 8. AGU, Washington, pp. 17–29.

Tsuya, H., 1955. Geological and petrological studies of volcano Fuji, V. Bulletin of the Earthquake Research Institute Tokyo, 33, 341-383.

Van Bemmelen, R.W., 1939. The volcano-tectonic origin of Lake Toba (North Sumatra). De Ingenieur in Nederlandsch Indie 6-9, 126-140.

Verhoogen, J., 1980. Energetics of the Earth. National Academy of Sciences, Washington DC.

Wadge, G., 1981. The variation of magma discharge during basaltic eruptions. Journal of Volcanology and Geothermal Research, 11, 139-168.

Wang, H.F., 2000. Theory of Linear Poroelasticity. Princeton University Press, Princeton.

Williams, H., McBirney, A.R., Lorenz, V. 1970. An Investigation of Volcanic Depressions. Part I. Calderas. Manned Spacecraft Center, Houston, Texas.

Wood, C.A., Kienle, J., 1992. Volcanoes of North America: United States and Canada: The United States and Canada. Cambridge University Press, Cambridge.

Woods, A.W., Huppert, H.E., 2003. On magma chamber evolution during slow effusive eruptions. Journal of Geophysical Research, 108, No. B8, 2403, doi: 10.1029/2002JB002019.

Yokoyama, I., 1957. Energies in active volcanoes. Bulletin of the Earthquake Research Institute Tokyo, 35, 75-97.